Technical Report 341

Radio-Echo Studies of Meteors at 68-cm Wavelength

Part II: Shower Meteors

J. V. Evans
R. A. Brockelman

15 January 1964

Prepared under Electronic Systems Division Contract AF 19(628)-500 by

Lincoln Laboratory
MASSACHUSETTS INSTITUTE OF TECHNOLOGY
Lexington, Massachusetts

The work reported in this document was performed at Lincoln Laboratory, a center for research operated by Massachusetts Institute of Technology, with the support of the U.S. Air Force under Contract AF 19(628)-500.

MASSACHUSETTS INSTITUTE OF TECHNOLOGY

LINCOLN LABORATORY

RADIO-ECHO STUDIES OF METEORS AT 68-cm WAVELENGTH

PART II: SHOWER METEORS

J. V. EVANS

R. A. BROCKELMAN

Group 31

TECHNICAL REPORT 341

15 JANUARY 1964

LEXINGTON MASSACHUSETTS

ABSTRACT

Radio-echo observations of five nighttime meteor showers are described. The observations were made at a wavelength of 68 cm and constitute part of a program of meteor observations carried out in the period 1960 to 1962 at the Millstone Hill Radar Observatory. The values for the velocities of the showers are presented and compared with values from other sources. The mean heights and trail lengths of these meteors are also given. Very precise velocity and deceleration measurements are presented for Quadrantid and Geminid meteors. These measurements were made by directing the radar beam along the path of the approaching meteors and determining the velocity directly from the doppler shift. These precise deceleration measurements are compared with the simple meteor theory for the case of free molecular flow. It is found that in a large number of cases the theory is inadequate and that cap formation for these meteors begins at heights somewhat above 100 km.

Accepted for the Air Force
Franklin C. Hudson, Deputy Chief
Air Force Lincoln Laboratory Office

TABLE OF CONTENTS

RADIO-ECHO STUDIES OF METEORS AT 68-cm WAVELENGTH

PART II: SHOWER METEORS

I. INTRODUCTION

Part I (Ref. 1) of this report described experimental studies of the radio reflection properties of sporadic meteors at a wavelength of 68 cm. In Part II, additional observations of five nighttime meteor showers are described. This work differs from that presented in Part I mainly in that the important results are relevant to the astronomy of meteors; whereas, the study of sporadic meteors gave useful results concerning the ion trails. One new kind of observation reported here is the measurement of the velocity of shower meteors traveling directly toward the radar. From these observations, accurate initial velocities v_∞ can be determined (by extrapolation), and the deceleration of the meteor in the earth's atmosphere can be measured with unprecedented accuracy. Thus, these particular results are capable of contributing to studies of the astronomy as well as the physics of meteors.

One of the ideas held by the authors at the commencement of this work was the possibility that the aspect sensitivity of meteor trails at this short wavelength (68 cm) might best be explored by observing meteor showers since they provide a fairly well collimated group of meteors having the same velocity. This concept was abandoned at an early stage when it was discovered[1] that low-velocity meteors possessed scattering patterns which were as narrow as the antenna beam (2.1° between half-power points), and probably as narrow as the angular distribution of radiant points in any of the showers investigated. Thereafter, shower meteors were studied chiefly in order to measure their velocities and decelerations.

At longer wavelengths ($\lambda \geqslant 3$ m), the principal meteor showers have been studied intensively, and a detailed review of this work together with the earlier visual and camera observations has been given by Lovell.[2] Since the method of measuring the velocity of a meteor employed in the work described here[3] is quite different from the widely applied Fresnel diffraction pattern method[4] (used at long wavelengths) it follows that any systematic errors possessed by the two methods should be different. Some discussion will be given of the values for the velocities of shower meteors obtained by the two methods.

II. EQUIPMENT

A brief description of the radar equipment has been given earlier.[1] As employed for observations of shower meteors it differed in no important respect from its use in the study of sporadic meteors (see Fig. 1 and Table I, Ref. 1).

TABLE I

OBSERVATIONS OF SHOWER METEORS

Shower	Date	Time (EST)	Tracking	Film	Comments
Orionids (1960)	21 Oct	0000–0400	Transits		DATA LOST DUE TO PUNCH FAILURE
	21–22 Oct	2320–0530	Transits		Only center part of filter bank on
	22–23 Oct	2240–0544	Transits		
Leonids (1960)	16–17 Nov	2245–0720	Transits	×	
	17–18 Nov	2330–0715	Transits		Camera jammed
Geminids (1960)	13–14 Dec	1820–1900	Radiant	×	First part of shower missed because of a blizzard
		1900–0100	Right-angle point	×	
		0350–0630	Right-angle point	×	Interruption for ABLE V track
Quadrantids (1961)	3 Jan	0000–1725	Right-angle point	×	
		1735–0035	Radiant	×	
	4 Jan	0035–0530	Right-angle point	×	
Perseids (1961)	11–12 Aug	1910–2000	Radiant	×	
		2000–2310	Right-angle point	×	Interruption for D-58 track (Trailblazer)
		2345–0700	Right-angle point	×	Tracking at proper azimuth
	12–13 Aug	1530–1930	Radiant	×	
		1930–0700	Right-angle point	×	Film not calibrated
Orionids (1961)	21 Oct	0020–0700	Right-angle point	×	
	21–22 Oct	2300–0310	Right-angle point	×	Interruption for satellite track
		0400–0620	Right-angle point	×	Film-time marks fogged
Leonids (1961)	17 Nov	0000–0600	Right-angle point	×	1° error in tracking
		0600–2400	Right-angle point	×	Proper tracking
	18 Nov	0000–1600	Right-angle point	×	Proper tracking; amplitude into computer via 5-kcps-bandwidth amplifier
Geminids (1961)	12 Dec	0015–0750	Right-angle point		
		0750–1015	Radiant		Amplitude into computer via 5-kcps-bandwidth amplifier
		1820–1910	Radiant		
		1910–0000	Right-angle point		
	13 Dec	0000–0750	Right-angle point		
		0750–1015	Radiant		Amplitude into computer via 5-kcps-bandwidth amplifier
		1820–1910	Radiant		
		1910–0000	Right-angle point		
	14 Dec	0000–0135	Right-angle point		Interruption for D-58 track (Trailblazer)
		0345–0750	Right-angle point		
		0750–1000	Radiant		
Quadrantids (1962)	2 Jan	1600–0000	Radiant		
	3 Jan	0000–1630	Right-angle point		Amplitude into computer via 5-kcps filter
		1630–0000	Radiant		
	4 Jan	0000–0800	Right-angle point		

III. OBSERVATIONS

Table I presents a list of the periods during which observations were made. At the commencement of the experiments unlimited observing time was available only during the nighttime hours; even then, conflicts with other site operations occasionally arose, as may be seen in Table I. Because of this only the following nighttime showers were investigated.

Quadrantids	(1961 and 1962)
Perseids	(1961)
Orionids	(1960 and 1961)
Leonids	(1960 and 1961)
Geminids	(1960 and 1961)

With the exception of the Perseids, all the reported meteor showers were observed in two succeeding years. We have previously described the detection scheme, data recording, and analyzing processes used in this work.[1] For the shower-meteor observations only one change was made. We took advantage of the aspect sensitivity of the trails to select shower meteors from the sporadic background (by continuously directing the antenna beam 90° from the position in the sky of the radiant point). In practice, this was accomplished by adjusting only the antenna azimuth and keeping the elevation fixed at 3° – a value which gave the largest amount of sky coverage consistent with freedom from refraction and interference effects. The beam azimuth was displaced from the azimuth of the radiant point by an amount which depended on the elevation of the radiant (Fig. 1). It is equally possible to use an antenna azimuth which is greater or smaller than that of the radiant point; this choice was taken to keep the antenna pointed in a southerly direction whenever possible. Auroral reflections could usually be seen to the north during at least some part of the night. During many of the early observations the antenna azimuth was adjusted to be exactly 90° from the azimuth of the radiant. This gave only approximate tracking of the

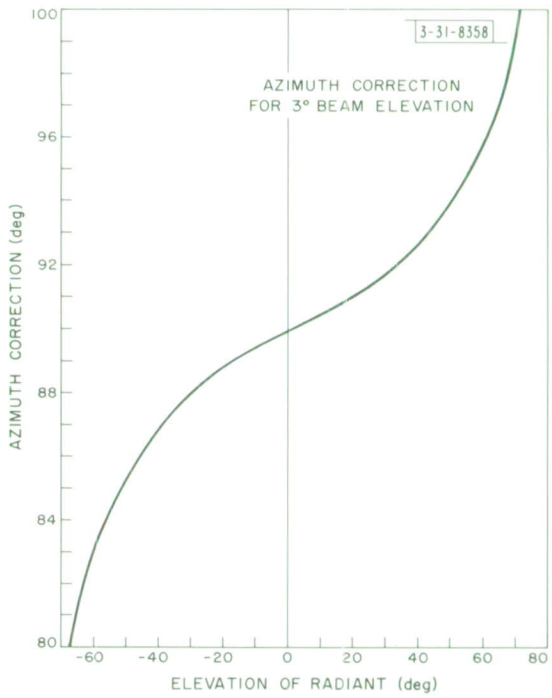

Fig. 1. Displacement of antenna azimuth from azimuth of radiant point as a function of the elevation of the radiant point. This displacement caused antenna beam to be directed at right angles to path of the meteors.

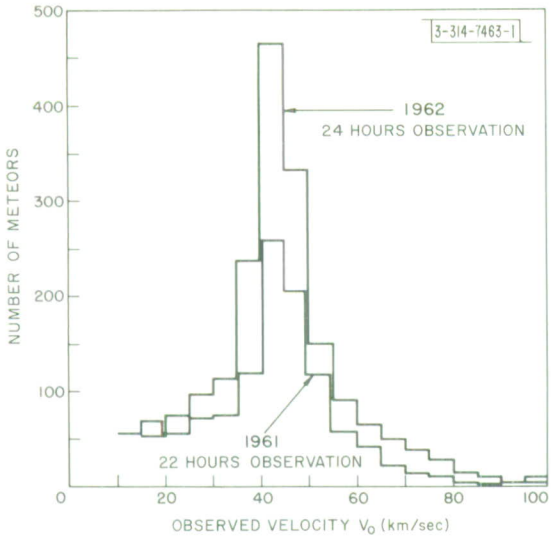

Fig. 2. Velocity distribution of meteors observed during Quadrantid meteor showers.

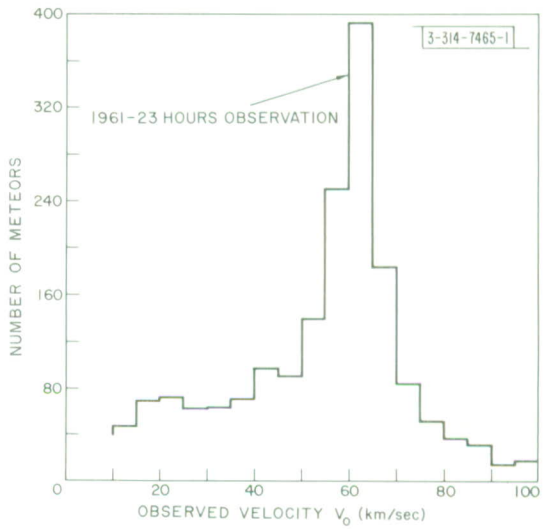

Fig. 3. Velocity distribution of meteors observed during the Perseid shower.

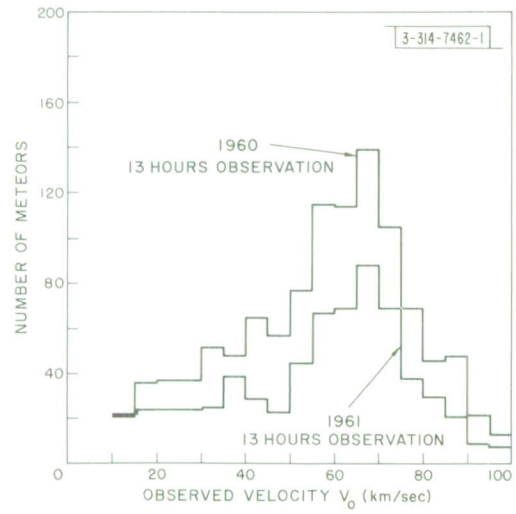

Fig. 4. Velocity distribution of meteors observed during Orionid showers.

optimum position and was later abandoned in favor of the more precise tracking afforded by following the curve shown in Fig. 1. The azimuth and elevation of the radiant point were computed in advance of the observation period (using the Millstone Hill CG 24 computer), from values for right ascension and declination of the radiants taken from sources such as Lovell[2] or McKinley.[5]

Quite early during the course of the observations of the 1960 Geminids attempts were made to observe meteors traveling directly toward the radar by pointing the antenna beam at the meteor radiant. These observations were expected to be successful only when the radiant point was low in the sky because the coverage provided by a 2° beam becomes vanishingly small for elevations greater than about 20°. Thus, most meteor radiants could only be observed while rising or setting. The Quadrantids, which are circumpolar at the latitude of Millstone Hill, were particularly suited for this type of study as the radiant was low in the north for long periods of time. For a meteor traveling directly toward the radar, the doppler shift encountered is far greater than that which will be accepted by the receiver filter bank ($>>25$ kcps). Thus, in these observations the receiver must be detuned from the transmitter frequency (by as much as 179 kcps in the case of the Perseids), to bring the center filter to the doppler shift expected for the particular shower being observed. This frequency offset was provided by a crystal-controlled oscillator so that the high-frequency stability of the system (nominally ~ 1 part in 10^{10}) was not seriously impaired. Toward the end of 1961 a frequency synthesizer became available which could perform the function of detuning the receiver whilst maintaining the absolute stability of the system equal to that of the master frequency standard.

In the sections to follow, results are presented for the determination of the velocities, heights, durations, intensities, and radial velocities of the meteors, in that order. The results of observations of meteors traveling toward the radar will also be presented.

IV. VELOCITIES

In this, and in the succeeding sections, the methods by which the data have been reduced are the same as those employed for the sporadic meteors[1] and will not be repeated. At the end of each period of observation the velocity of each meteor was computed and histograms were drawn showing the number of meteors observed in each 5-km/sec interval from 10 to 100 km/sec. Figures 2 through 6 show the histograms obtained following observations of the five meteor showers listed in Sec. III. When these histograms are compared with Fig. 7, which gives the average distribution of the velocities of sporadic meteors observed during the nighttime, it becomes evident that a substantial number of shower meteors were observed in every case. Particularly striking are the large numbers of Quadrantid meteors seen in 1962 and Geminids in 1961. It is probably true to say that although much larger numbers of meteors have been observed with long-wave radar equipment, never have so many observations been reduced to give velocity measurements during a single shower.

In order to obtain a more precise estimate of the velocities of these showers, the histograms (Figs. 2 to 6) have been replotted in 1-km/sec steps (Figs. 8 to 12). These expanded plots show that for the Geminids, Quadrantids, and Perseids (where the percentage of shower meteors was high) the distribution of velocities is Gaussian so that a mean and a standard deviation may easily be computed. A constant number of meteors was subtracted from each 1-km/sec interval (Figs. 8, 9, and 12) to remove the sporadic background. The values obtained from this work are given

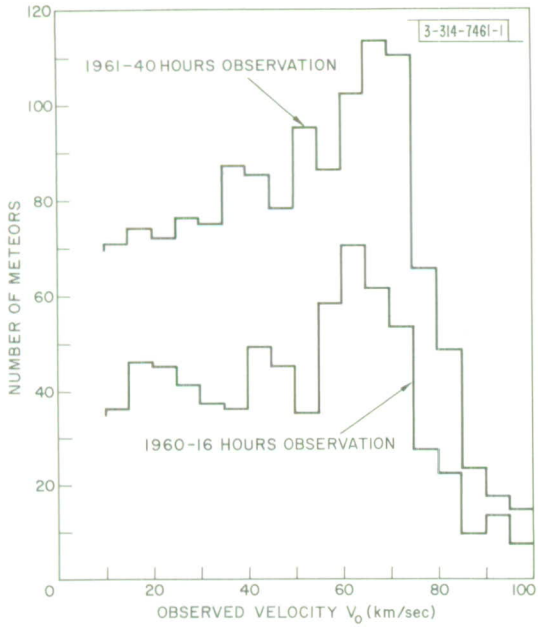

Fig. 5. Velocity distribution of meteors observed during Leonid showers.

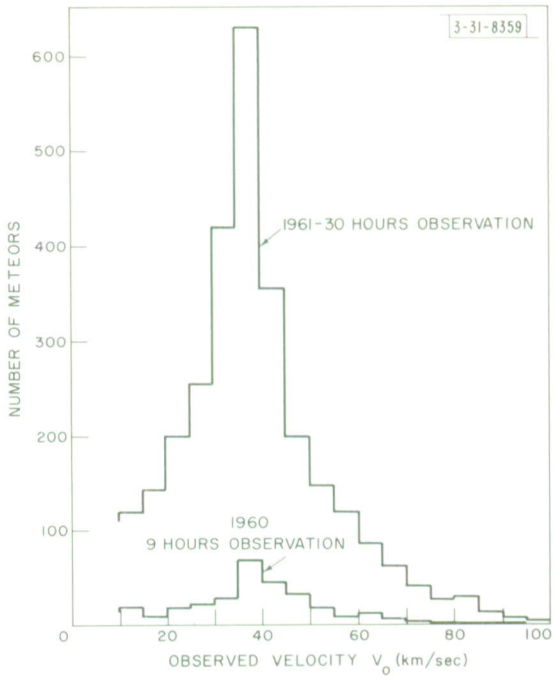

Fig. 6. Velocity distribution of meteors observed during Geminid showers.

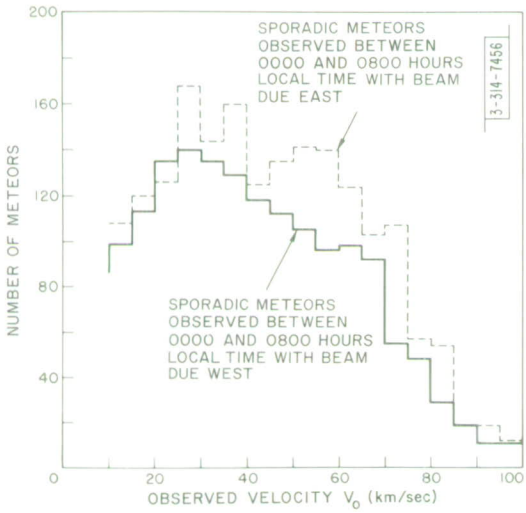

Fig. 7. Distribution of sporadic meteor velocities observed at night.

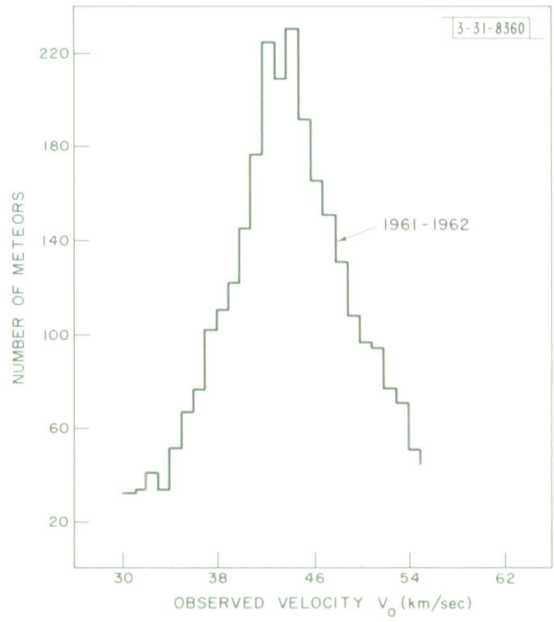

Fig. 8. Observed distribution of velocities of Quadrantid meteors.

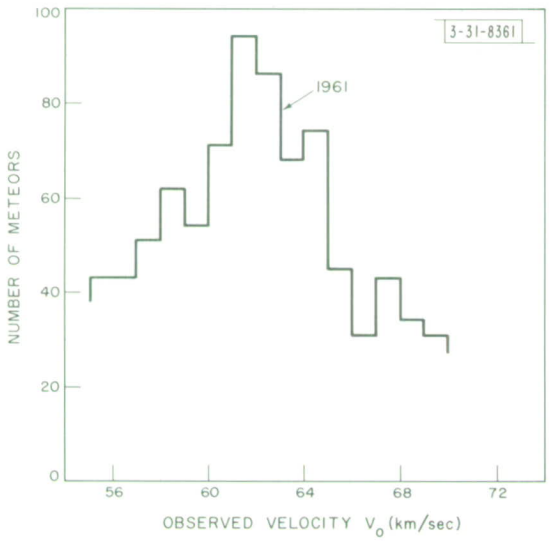

Fig. 9. Observed distribution of Perseid meteors.

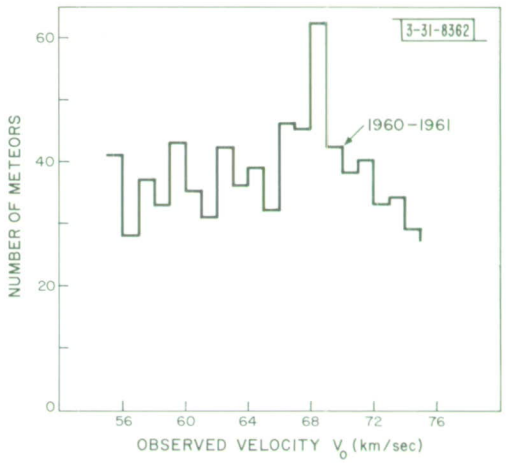

Fig. 10. Observed distribution of Orionid meteors.

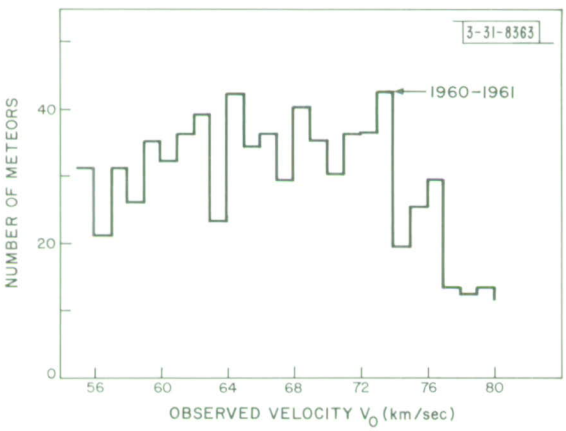

Fig. 11. Observed distribution of Leonid meteors.

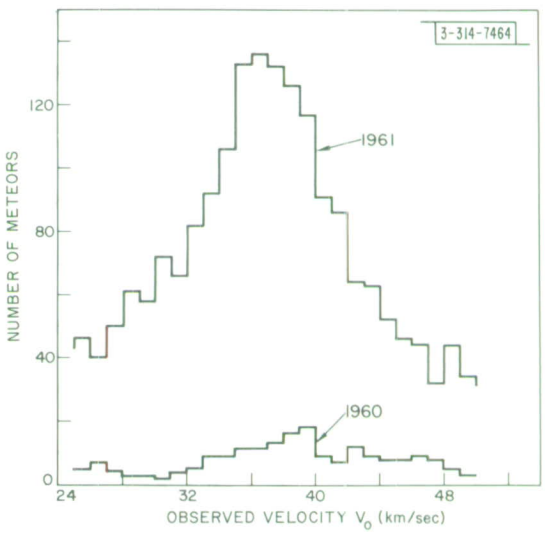

Fig. 12. Observed distributions of Geminid meteors.

TABLE II

VALUES OF OBSERVED METEOR VELOCITIES v_o (km/sec)

Shower	This Paper	This Paper After Doppler Restriction	McKinley*	Hawkins and Almond†
Geminids	36.46 ± 4.59 (1115 meteors)	36.51 ± 2.56 (413 meteors)	35.0	35.7 ± 4.6
Quadrantids	43.98 ± 4.26 (1329 meteors)	43.17 ± 4.63 454 meteors)	41.0	38.5 ± 3.4
Perseids	61.68 ± 2.20 (344 meteors)	62.36 ± 2.31 (100 meteors)	60.0	60.5 ± 4.6
Leonids	69.0 (196 meteors)		72.0	
Orionids	69.9 (600 meteors)		66.0	

* See Ref. 5.

† See Ref. 6.

in Table II. The velocities for the Leonids and Orionids were estimated from the 5-km/sec-interval plots (Figs. 4 and 5) – a procedure which is somewhat complicated by the fact that these showers fall on the sloping part of the sporadic background distribution.

Also given in Table II are values presented by McKinley,[5] Hawkins and Almond[6] for the velocities of these showers obtained by radio-echo methods. In general, it appears that the values presented here are higher than those obtained by the use of long-wave radar equipment. This is caused in part by systematic errors in the results which tend to increase v_o together with errors in the long-wave measurements which serve to decrease v_o. The errors in the long-wave measurements are brought about by meteor deceleration which displaces the maxima and minima in the Fresnel amplitude pattern in such a way that too low a value of v_o will be obtained. At least two sources of systematic error are believed to exist in the measurements described here. Potentially, the most serious error is an over-estimation in the range R caused by the mismatch between the 1-msec pulses and the filters in the receiver, which are designed for 2-msec pulses. That is, the peak signal appearing at the output of these filters does not occur 1 msec after the pulse has been applied, but at some later time. Controlled measurements were made of this effect to obtain a correction, which was then uniformly applied to correct the range data for both the sporadic and the shower meteors. Unfortunately, the amount of delay introduced by the filters seemed to depend upon the signal-to-noise ratio and, hence, it was possible to correct accurately only for signals of a given intensity. If no correction is made then the overestimate of the range will lead directly to a velocity which is too high by virtue of the equation for velocity

$$v_o^2 = R\ddot{R} + (\dot{R})^2 - x\ddot{x} \quad , \tag{1}$$

where v_o is the observed meteor velocity, R is the meteor range, and x is the distance of the meteor from the point on the trail where a line drawn to the radar intersects perpendicularly.

The second systematic error is omission of the deceleration factor, i.e., the term $x\ddot{x}$, which also serves to cause v_o^2 to be overestimated. However, this term is generally small because meteors are seen close to the normal to the trail where x is small. By restricting the sample of meteors to those in which $\dot{R}$ is very small ($\pm 1/2$ km/sec) one can insure that x is small (< 10 km) and thereby minimize the error from this source. This has been done for three of the showers and the results are presented in column 3 of Table II. It is evident that despite this selection the observed velocities are still high and that the difference between these and the long-wave radar velocities appears to increase with velocity, although it never becomes larger than the standard deviation. For the Perseids, the difference between the long-wave and these short-wave measurements amounts to 3 percent. It may be shown that the term $x\ddot{x}$ ($x \sim 10$ km, $\ddot{x} \sim 1$ km/sec^2) is only of the order of 0.3 percent of v_o^2 for this selected group of meteors.

The geocentric velocity v_g of a meteor at the earth's distance from the sun will be the vector sum of the earth's orbital velocity v_e (lying between 41.4 and 42.8 km/sec depending upon the time of year), and the heliocentric velocity of the meteor v_h. The velocity of the meteor as observed in the earth's atmosphere v_o will differ from v_g for three reasons:[2,5]

(a) Gravitational attraction. The meteor will be accelerated by the earth's gravitational field and will acquire an additional velocity component such that before entering the earth's atmosphere its velocity v_a is

$$v_a^2 = 124.9 + v_g^2 \quad . \tag{2}$$

This effect also shifts the apparent position of the radiant and is frequently described as zenith attraction.

(b) Diurnal aberration. Due to the rotation of the earth, an observer has an additional component of velocity of 0.464 cos (lat) km/sec, which is added vectorally to the meteor velocity. For Millstone, this correction cannot exceed ± 0.33 km/sec and has been omitted. However, where it is included, v_a will be modified and the resulting velocity v_∞ is that which an observer would see if there were no atmosphere.

(c) Atmospheric deceleration. When the meteor encounters the drag imposed by the earth's atmosphere its momentum provides the necessary energy to overcome the drag and consequently it is slowed down (at the rate of ~ 1 km/sec). Thus, the observed velocity v_o will in general be less v_∞.

Values for v_∞ obtained from photographic work are probably the most precise measurements of meteor velocities presently available. Two sets of values taken from survey papers[7,8] are given in Table III. It can be seen that the values for v_o given in Table II obtained in this paper are in fact higher than the accepted values of v_∞. Thus, it is not possible to argue that these short-wave values of v_o differ from the long-wave measurements because they are less influenced by deceleration (by assuming that the echoes are largely from the early part of the trail). Evidently, there remains a systematic error that has not been allowed for.

During the three major showers, meteors were observed traveling directly toward the radar. In these studies, the velocity is given directly by the doppler shift, and each echo provides an independent measurement. This work is presented in Sec. IX-B, but here it is pertinent to note

TABLE III

VALUES OF EXTRAPOLATED METEOR VELOCITIES v_∞ (km/sec)

Shower	This Paper	Whipple and Hawkins*	Mean of Values Given in Hawkins and Southworth†
Geminids	36.55 (36.73)‡	36.5	36.2
Quadrantids	42.42 (42.46)‡	42.7	42.6
Perseids	~60.26	60.4	60.6

* See Ref. 7.

† See Ref. 8.

‡ Values obtained from the curve-fitting procedure described in Sec. IX-D and presented in Table XI.

that values for v_∞ could be obtained from these measurements by extrapolation. They are presented in Table III. Good agreement is found with the photographic values. The scatter of values in the three major showers is given almost exclusively by the real spread in velocities and not by the errors of measurement. This agreement suggests that the measurement of radial velocity $\dot{R}$ in Eq. (2) is not a source of error. The measurement of the range R is, perhaps, responsible for the systematic errors in the values of v_o – due possibly to improper correction for the large delays in the receiver.

In summary, we may say that the values reported here for the meteor-shower velocity in the earth's atmosphere v_o have rms errors comparable to those found in the long-wave radar measurements, but suffer from different systematic errors. The measurements of the velocities of meteors traveling directly toward the radar, however, yield values of v_∞ at least as good as the best photographic determinations.

V. DURATIONS

As defined in Ref. 1, the term "duration" used here denotes the time interval between the receipt of the first and last echo. Because most meteors are seen traveling perpendicular to the beam, the duration can be interpreted as a measure of the over-all length of the trail. The finite width of the beam changes both the distribution of the lengths observed and the mean length. However, after allowance for this effect it has been found that the distribution of the lengths ℓ of the sporadic meteors is given by

$$n_\ell \propto \exp[-\ell/\ell_o] \tag{3}$$

where the scale length ℓ_o is of the order of 6 km. Plots of the distribution of the durations observed for the five nighttime showers are given in Figs. 13 to 17. In all cases, the distribution conforms to the law observed for the sporadic meteors, namely,

$$n_t \propto \exp[-t/T] \tag{4}$$

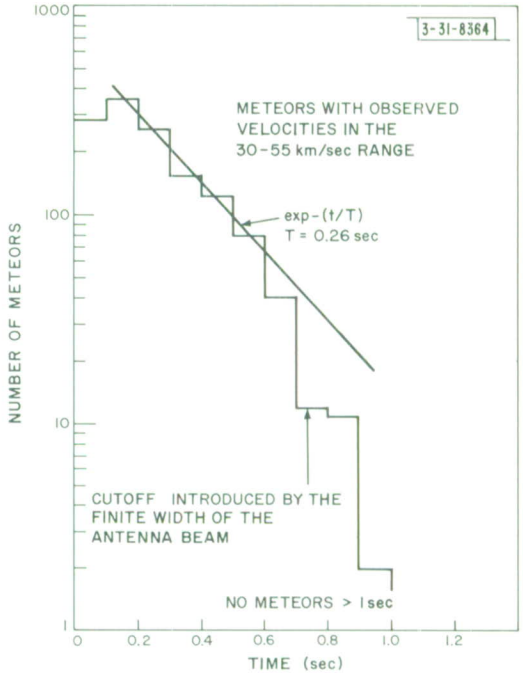

Fig. 13. Duration distribution observed for Quadrantid meteors (1962).

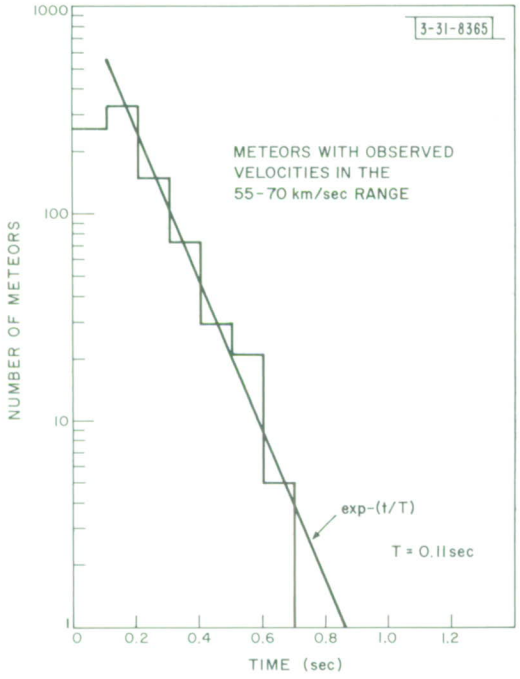

Fig. 14. Duration distribution observed for Perseid meteors (1961).

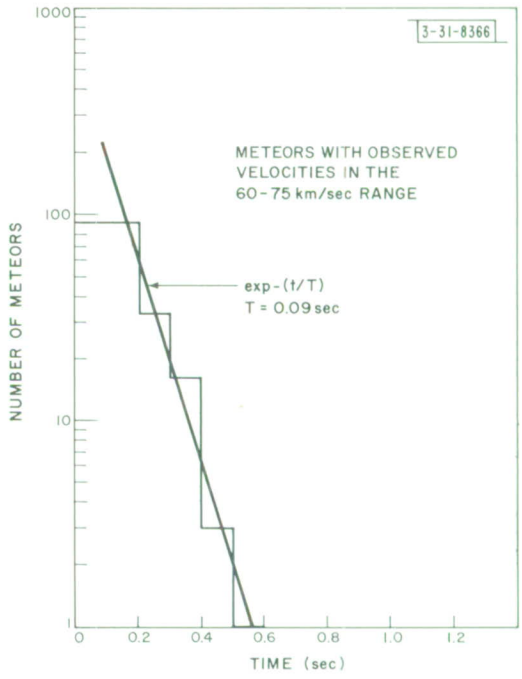

Fig. 15. Duration distribution observed for Orionid meteors (1961).

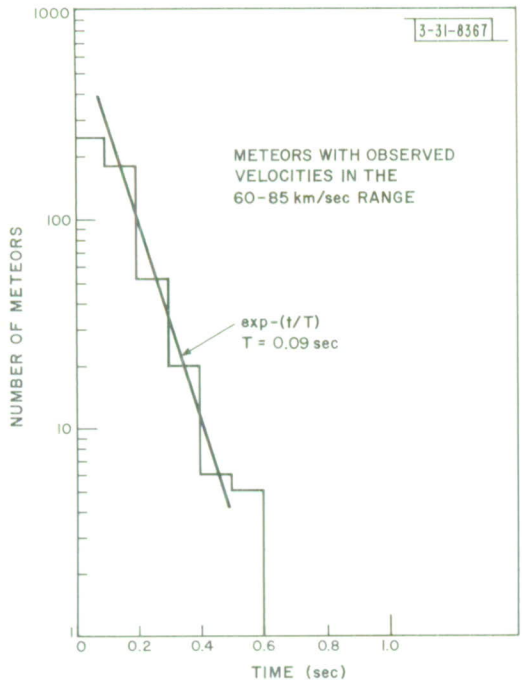

Fig. 16. Duration distribution observed for Leonid meteors (1961).

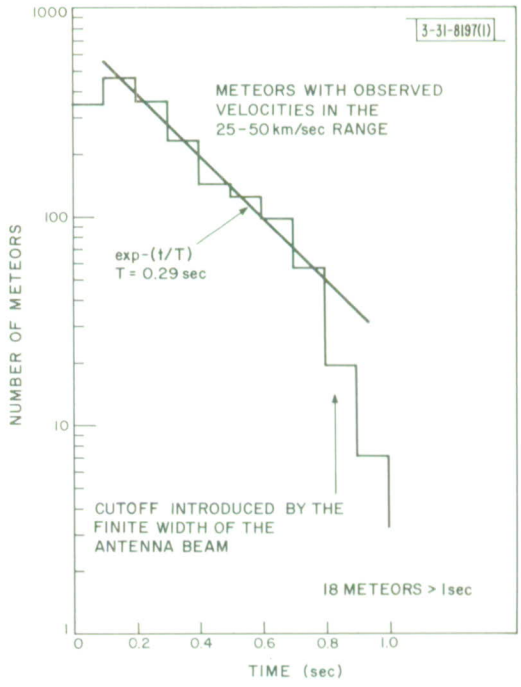

Fig. 17. Duration distribution observed for Geminid meteors (1961).

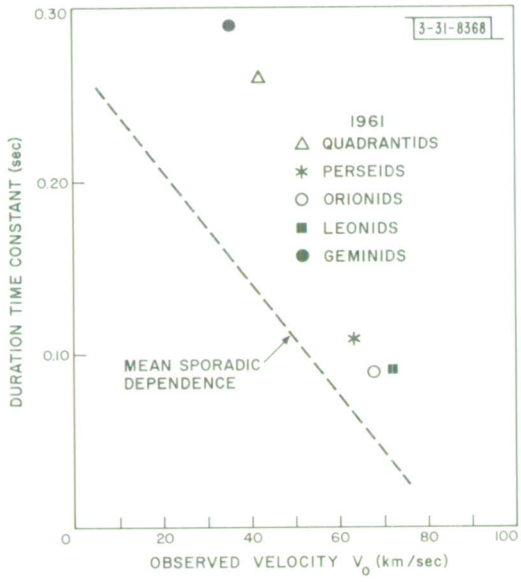

Fig. 18. Values of duration time constant T plotted as a function of velocity.

For the Quadrantids (Fig. 13) and Geminids (Fig. 17), there is a noticeable cutoff introduced by the finite width of the antenna beam (~30 km). It appears that for these showers a substantial number of meteors completely traverse the beam. Such a striking cutoff in the duration distribution was not observed for the sporadic meteors, implying that the Quadrantids and Geminids have trail lengths which are longer than the average sporadic meteor trail. The values for the duration time constant T are plotted in Fig. 18 together with the variation of this quantity observed for the sporadic meteors. It may be seen that in all cases the duration time constant T for the shower meteors is higher than that for sporadic meteors of the same velocity. This implies that in all cases the trail lengths are longer than those of sporadic meteors. As noted above, this is particularly striking in the case of the Geminid and Quadrantid meteors. If we represent the observed distribution n_z of trail lengths in

$$n_z \propto \exp[-z/z_o] \quad , \tag{5}$$

then the scale length z_o is given by the product $v_o T$. Table IV lists these values.

As mentioned above, the finite width of the antenna beam causes the observed distribution of trail lengths [Eq. (5)] to differ from the true distribution. This point has been considered in some detail by T. Hagfors in Appendix 1, Ref. 1. Hagfors assumed that the true distribution of trail lengths ℓ was of the form given in Eq. (3) and computed the expected distribution which would be observed for three cases (where ℓ_o equals 15, 10, and 6 km). These results are presented in Fig. 3(a-c) in the Appendix of Ref. 1. In each case, the observable distribution is approximately of the form given in Eq. (5) where the values of z_o are 9.75, 7.35, and 5.02 km, respectively. That is, the narrow antenna beam does not seriously alter the form of the distribution of trail lengths but does tend to steepen it.

Making use of Fig. 4 of the Appendix,[1] we have obtained values for ℓ_o corresponding to the observed values of z_o for the five showers. These are given in Table IV. The shower meteors exhibit larger values of ℓ_o than observed for the sporadic meteors, implying that their average trail lengths $\bar{\ell}$ are longer also. In practice, the true mean length is given approximately by the

TABLE IV
TRAIL LENGTHS

Shower	Observed Scale Length z_o (km)	True Scale Length ℓ_o (km)	Mean Length of Photographic Meteors (km)
Quadrantids	10.9	18.0	12.6 (5 meteors)
Perseids	6.6	8.6	13.8 (9 meteors)
Orionids	5.9	7.4	14.6 (12 meteors)
Leonids	6.5	8.4	
Geminids	10.4	16.6	12.8 (16 meteors)
Sporadics	4.7	5.6	8.0-15.0 (depending upon velocity)

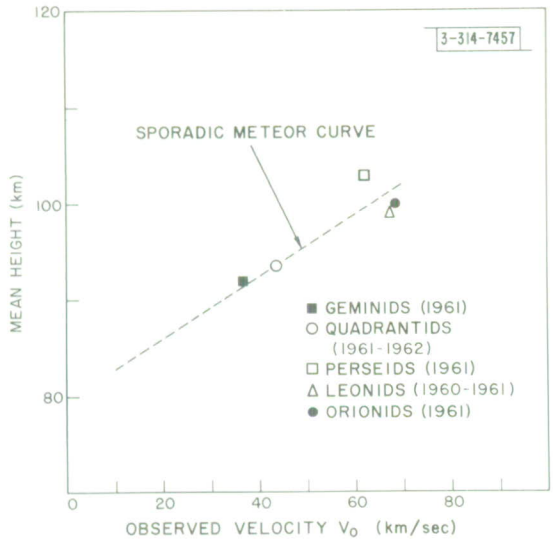

Fig. 19. Values of mean height of the five showers as a function of velocity.

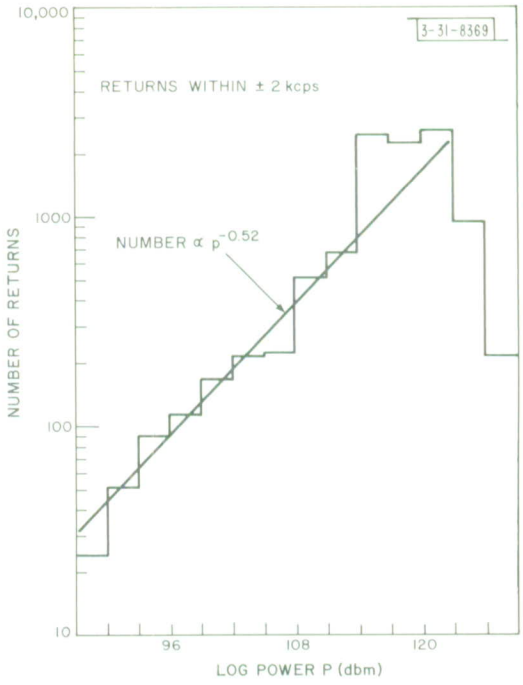

Fig. 20. Distribution of echo powers for Leonid meteors (1961).

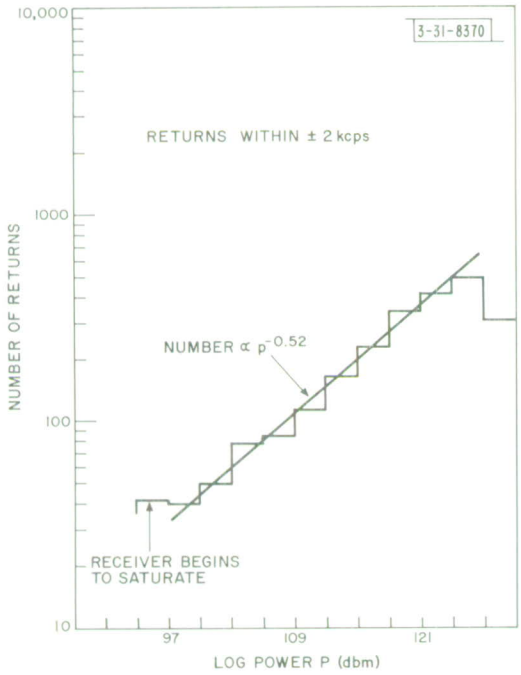

Fig. 21. Distribution of echo powers for Geminid meteors (1961).

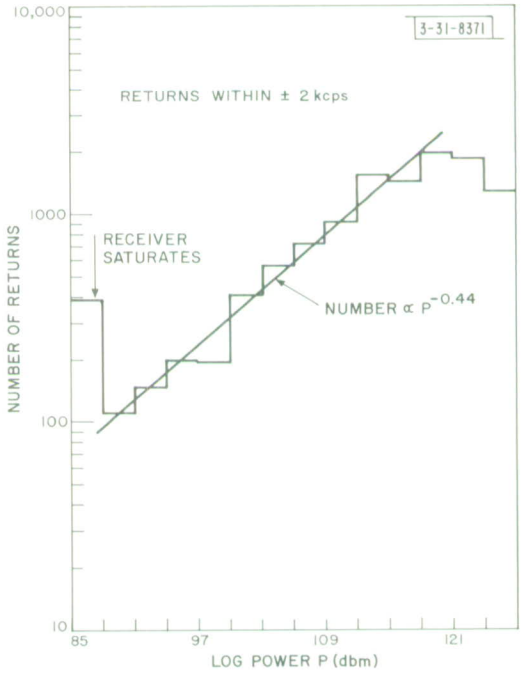

Fig. 22. Distribution of echo powers for Quadrantid meteors (1962).

scale length ℓ_o and hence column 3 of Table IV may be taken as representing the mean lengths $\bar{\ell}$ of the trails of the meteors in these showers. Comparison lengths have been obtained from Hawkins and Southworth[8] who published beginning and end heights of photographic meteors brighter than +4.5 magnitude. The photographic shower meteors exhibit lengths which are not noticeably different from the mean lengths of the sporadic meteors at the same velocity. This is not the case for the radio meteors presented here. We suggest that the difference stems from the different limiting magnitudes (+4.5 photographic, +8.0 radio) of the two surveys. The shower meteors possess more bright members than the sporadics and, thus, with equipment which can detect meteors down to a high enough limiting magnitude, one might expect a significant difference in the mean lengths of the shower and sporadic meteors.

VI. HEIGHTS

The mean heights of the five showers (plotted as a function of velocity), together with the variation observed for the sporadic meteors are shown in Fig. 19. The Geminid and Quadrantid showers fall close to the sporadic curve indicating that the composition of these two showers cannot be very different from that of the sporadic meteors. The Perseids, on the other hand, fall well above the sporadic curve, supporting the view that this shower contains many meteors of very low density.

VII. INTENSITIES

Distributions of the number of returns vs intensity were obtained only during the Leonids (1961), Geminids (1961), and Quadrantids (1962). These are shown in Figs. 20 to 22. In Ref. 1 we found that for sporadic meteors the number of returns n_p with power p was given in

$$n_p \propto p^{-0.63} \quad , \tag{6}$$

and also that the number with a cross section σ was given in

$$n_\sigma \propto \sigma^{-0.63} \quad . \tag{7}$$

The exponent observed for the shower meteors is in all cases lower than the exponent observed for sporadic meteors, indicating a higher proportion of bright meteors. The higher incidence of bright meteors in showers might be a consequence of the Poynting-Robertson effect as suggested by Kaiser.[9] According to Whipple and Hawkins[7] few photographic meteors are of asteroidal origin and most shower meteors are certainly associated with comets. Thus, the distinctly different behavior of meteors in certain streams perhaps reflects differences in the constitution of the parent comet and its subsequent history.

The number of meteors with mass m is usually expressed in the form

$$n_m \propto m^{-s} \quad , \tag{8}$$

and since meteor theory[5,10] leads to the result that the electronic line density in the trail is proportional to the mass m, we should expect that the number of meteors n_q observed with line density q to be

$$n_q \propto q^{-s} \quad . \tag{9}$$

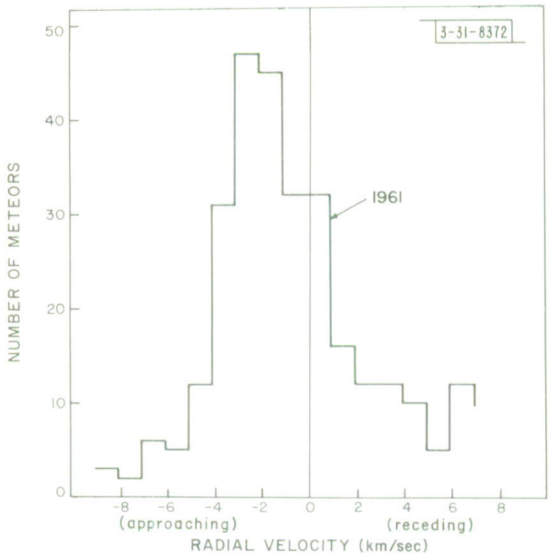

Fig. 23. Distribution of mean radial velocities observed for the Orionid meteors (1961); asymmetry of peak is due to improper tracking of radiant point.

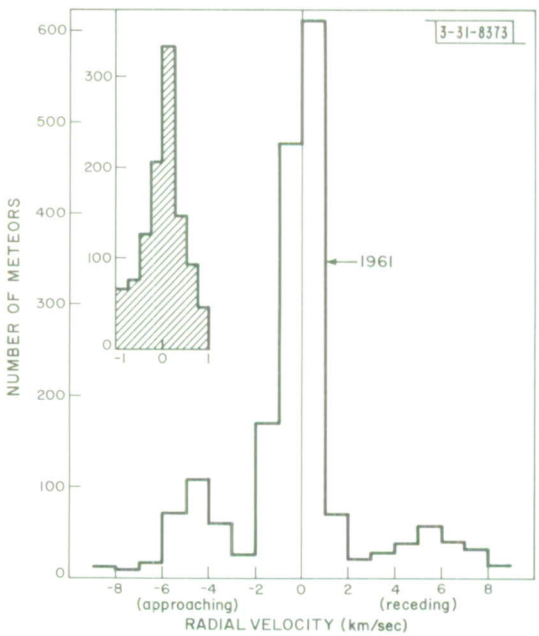

Fig. 24. Distribution of mean radial velocities observed for Geminid meteors (1961). (In this case tracking was proper.) Also, meteors appear to have been observed in the main sidelobes of the antenna providing further evidence of long trails produced by the meteors in this shower.

The scattering from these meteor trails is almost certainly coherent. Incoherent scattering can be ruled out because extremely large line densities ($q > 10^{20}$ electrons/meter) would be required to explain the observed cross sections. Thus, we expect that the echo power will vary as the square of the line density q; therefore, the distribution of echo powers will be

$$n_p \propto p^{-s/2} \quad . \tag{10}$$

From this we conclude that for the sporadics s = 1.26, the Geminids and Quadrantids s = 0.88, and the Leonids s = 1.04. The accepted values[5,9,10] for meteors with visual magnitude in the vicinity of +7 are: sporadics s = 2.0; Geminids s = 1.6 – 1.7; and Quadrantids s = 1.7 – 1.8. Thus, there is agreement that the showers contain a higher proportion of bright meteors, but total disagreement on the value for s. We have suggested (see Ref. 1) that this arises as a consequence of the fact that many of these meteors suffer fragmentation. As a result of the fragmentation the simple assumption that the line density is proportional to the mass breaks down. In long-wave radar observations the echo comes from a cylindrical column of ionization which may be of the order of several kilometers long. It follows that short period fluctuations of the line density tend to be averaged out and, hence, such observations are somewhat less influenced by this effect. In conclusion we consider that it is not possible to determine the mass distribution laws, i.e., the true values for s in Eq. (8), for either sporadic or shower meteors in these observations unless some selection procedures can be found to eliminate those meteors which suffer fragmentation. However the mass laws obtained might then not be representative.

VIII. RADIAL VELOCITIES

The measurement of the radial velocity of the sporadic meteors provided a means of examining the aspect sensitivity of the ion trails. This is not possible in the case of shower meteors for they do not enter the antenna beam in a random fashion. However, it is possible (at least in principle) to determine the radiant point of a meteor shower by means of a narrow beam antenna. A demonstration of this is given in Figs. 23 and 24. During the Orionid shower in 1961, the tracking of the radiant point was imprecise because the curve of Fig. 1 was not followed. Instead, a fixed displacement of 90° between the azimuth of the antenna and the azimuth of the radiant was employed. Because the observations were made when the radiant was above the horizon, a displacement of 90° was insufficient and the shower meteors passing through the beam had (as expected) a component of velocity in a direction towards the radar. This is evident in Fig. 23. Since the tracking was precise during the Geminid shower the mean radial velocities are symmetrically arranged about zero (Fig. 24). Also of interest in Fig. 24 are the minor peaks on either side of the principal one, which are thought to represent meteors observed in the sidelobes adjacent to the main beam. The spacing of these peaks is correct according to the antenna pattern measurements of Fritsch.[12] Such sidelobes were not identified at any other time. One would not expect to observe them when studying the sporadics since they may enter the beam at a wide variety of angles. Two factors which may account for why this effect was observed for the Geminids are offered. According to Lovell[2] both the Perseid and Quadrantid radiants are broadly distributed. The Quadrantid radiant is complex and apparently covers a wide area (at least 20° in diameter). The Perseid radiant is diffuse with a diameter of 10° to 15°. The Geminids, on the other hand, have a diameter of ~12° with a concentration in a region 4° × 3°. Thus, perhaps, the Geminids are the best collimated group of meteors that have been observed

and, therefore, intercept the antenna beam along paths which are the most nearly parallel. This is an important requirement if the influence of the antenna pattern is to be observed. Since the sidelobe levels are ~20 db below the main beam, a second requirement is a very high percentage of bright meteors. Figure 21 indicates that this requirement is also satisfied for the Geminids.

In all cases where the antenna steering is thought to have been performed properly, the distribution of mean radial velocities was symmetric about the zero position. Thus, to the accuracy of these observations (which is very poor in declination), the radiant positions given by Lovell[2] and McKinley[5] are found to be correct.

IX. METEORS TRAVELING DOWN THE BEAM

A. Observations

By directing the antenna beam toward the radiant point and detuning the receiver to compensate for the large value of doppler shift corresponding to an approaching meteor, it has been possible to observe meteors traveling radially toward the radar. Periods when this was attempted are shown in Table II where the antenna tracking is labeled "radiant." These observations were only attempted for the Quadrantids, Perseids, and Geminids. With a narrow (2°) beam, the amount of sky through which a shower meteor may pass and give rise to an echo is reduced in the "radiant" tracking position by about a factor of ten from that in the "right-angle" point position. At elevations greater than 3°, the useful area is still further reduced, and it was considered worthwhile directing the antenna at the radiant only when the radiant elevation was below about 20°. An additional reduction in the rate could be expected to arise as a result of the reduced cross section of the meteors when observed "head on." (The rates observed for these three major showers were in fact reduced to the order of 2 shower meteors per hour.) Thus, for successful observations of meteors traveling toward the radar, one requires a strong shower having a radiant whose declination is substantially different from the latitude of the observer. The radiant will then rise and set slowly, thus spending a long period of time at low elevations. The Orionids and Leonids were unsuitable on both these counts and no attempts were made to observe meteors traveling down the beam during these showers.

The separation of the meteors traveling directly down the beam from those which traverse it at a grazing angle proved less difficult than anticipated. In the first place, with the receiver detuned such that the center filter of the doppler filter bank corresponds to the frequency of an approaching shower meteor (with velocity v_s), meteors traveling radially toward the radar only in the range $v_s \pm 9$ km/sec can be detected. Any meteor with velocity v (measured in km/sec) traversing the beam at an angle φ to the axis will only be detected when the relation

$$\cos^{-1}\left(\frac{v_s + 9}{v}\right) \leq \varphi \leq \cos^{-1}\left(\frac{v_s - 9}{v}\right) \tag{11}$$

is satisfied. All other things being equal, one would expect to observe more meteors for which $v > v_s$ than $v < v_s$. Yet, because the available number of sporadic meteors decreases as $v \geq 40$ km/sec (see Fig. 7), the net effect will be an extremely large reduction in the rate of sporadic meteors when the receiver is detuned. Three tests are then applied to select meteors traveling toward the radar:

(1) The duration should be large. A minimum value of about 0.5 sec was taken.

(2) The velocity computed in the normal way (v_o) should be close but somewhat greater than the mean radial velocity. The velocity computed using Eq. (1) is expected to be higher than the mean radial velocity due to the omission of the term $x\ddot{x}$ (which will now be large).

(3) The mean rate of change of radial velocity must be small ($< 2\,km/sec^2$).

Figure 25 shows a scatter diagram for the meteors observed during the Geminid shower in 1961. Conditions (1) and (2) suggest that the cluster of long-duration meteors centered on 36-km/sec radial velocity and 42.5-km/sec "observed" velocity v_o are Geminids. By applying condition (3) we can confirm this, and in Fig. 26 we plot mean radial velocity vs the mean derivative of the radial velocity and find a distinct group of meteors with long durations centered on a mean radial velocity of 35.5 km/sec and $1\,km/sec^2$ mean deceleration. The members of this group were accepted as Geminids and all others rejected, although in fact some of those shown in Fig. 26 might also have been Geminids. A similar selection procedure was employed for the Quadrantids and Perseids, although here the problem was made much easier by the higher value of v_s and correspondingly lower number of sporadic meteors observed.

These procedures will not preclude the acceptance of a meteor traveling at a small angle (less than, say, 5°) to the axis. Thus, the angular extent of the radiant will play some part in limiting the accuracy obtained by this technique.

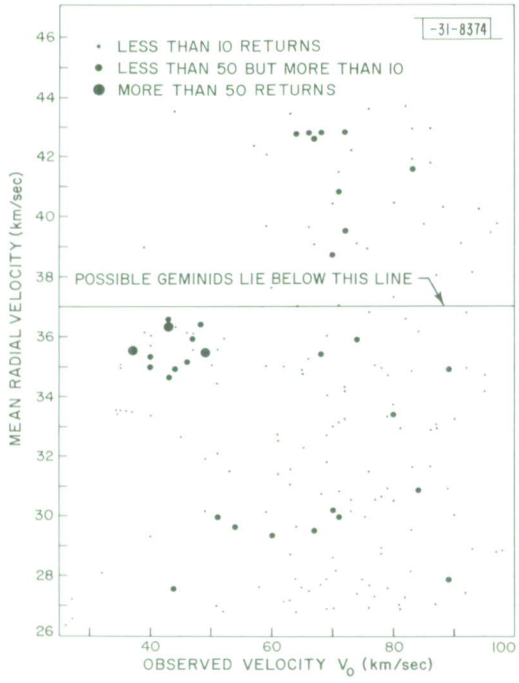

Fig. 25. Mean radial velocity shown as a function of computed velocity for each meteor observed during the period when a search was made for Geminid meteors traveling along paths directly toward the radar (1961).

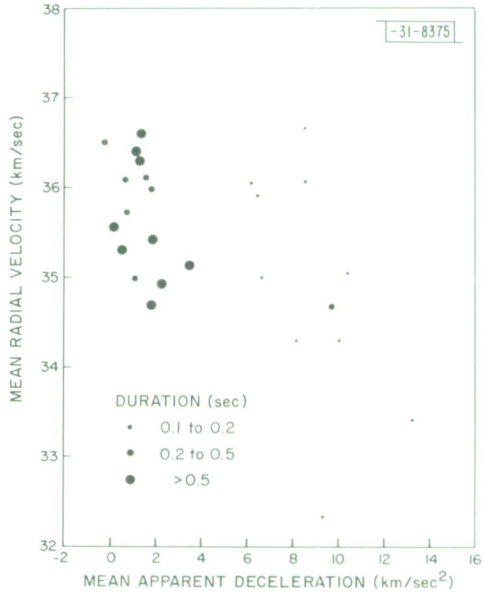

Fig. 26. Mean radial velocity of meteors (Fig. 25) plotted against mean apparent deceleration. The members of this group which have long durations are believed to be Geminids.

B. Results

Velocities:– Tables V to VII summarize the results of these observations. In the case of the Perseids (Table V) the durations were mostly shorter than the Geminids (Table VI) and Quadrantids (Table VII). In general, the Perseid meteors showed little or no evidence of deceleration but gave a somewhat wider scatter of values for the radial velocity than the Geminids or Quadrantids. An example of this is presented in Fig. 27 where the radial velocity is plotted as a function of time for Perseid 7. Thus, the extrapolated velocities v_∞ for these meteors cannot reliably be obtained. We attribute this behavior to the apparent ability of the Perseids to fragment readily.

For most of the Geminids and Quadrantids, the radial velocity showed a smooth uniform decrease with time. Representative examples are given in Figs. 28 to 34. Where the duration exceeded about 0.75 sec, a smooth curve was fitted to the points and extrapolated backwards in time until the gradient of the curve became zero. The velocity at which this occurred is given in the fourth column of Tables V to VII as v_∞ together with an estimate of the accuracy of this value. Weighted mean values for v_∞ are given in Tables VI and VII. The mean velocity given in column 3 of Table V may be taken as the lower limit of v_∞ for the Perseids. As remarked in Sec. IV these values are in close agreement with values for v_∞ obtained from photographic work.

TABLE V

PERSEIDS (1961)

Number	Date	Start Time (EST)	Observed Initial Velocity*	v_∞ (extrapolated)	Duration (sec)
1	13 Aug	1536.56	60.003	60.003	0.59
2	13 Aug	1546.27	59.953		0.30
3	13 Aug	1607.28	60.469		0.74
4	13 Aug	1620.56	60.089		0.34
5	13 Aug	1733.51	59.317		0.24
6	13 Aug	1835.52	59.503		0.52
7	13 Aug	1841.25	60.534		1.37
8	13 Aug	1844.20	59.812		0.32
9	13 Aug	1905.15	60.693		0.58
10	13 Aug	1912.32	59.848		0.28
11	13 Aug	1917.16	60.134	~60.53	0.49
			Mean values = 60.032	60.26	

* Mean of first 6 returns.

TABLE VI

GEMINIDS (1961)

Number	Date	Start Time (EST)	Observed Initial Velocity*	v_∞ (extrapolated)	Duration (sec)
1	12 Dec	0819.33	35.028		0.40
2	12 Dec	0825.26	35.605	35.70 ± 0.05	1.08
3	12 Dec	0827.25	34.921		0.56
4	12 Dec	0827.28	35.840	36.6 ± 0.20	0.92
5	12 Dec	0844.28	35.723		0.55
6	12 Dec	1006.41	36.731	36.72 ± 0.05	0.85
7, 8	12 Dec†	1829.34	36.209		1.06
9	12 Dec	1907.17	36.781	36.80 ± 0.05	1.39
10	13 Dec	0917.31	35.396		0.62
11	13 Dec	1801.47	36.475	37.2 ± 0.20	1.97
12	13 Dec	1833.40	36.41		0.53
13	13 Dec	1904.48	36.936	37.0 ± 0.05	1.17
14	13 Dec	1927.16	36.441		0.27
15	14 Dec	1941.21	35.217	35.80 ± 0.20	2.78
		Mean values =	35.979	36.55	

* Mean of first 6 returns.

† This meteor appears to have fragmented into two pieces.

TABLE VII

QUADRANTIDS (1962)

Number	Date	Start Time (EST)	Observed Initial Velocity*	v_∞ (extrapolated)	Duration (sec)
1	2 Jan	1714.02	42.357	42.90 ± 0.10	0.72
2	2 Jan	1839.00	42.598	42.64 ± 0.05	0.87
3	2 Jan	2047.54	43.189	43.32 ± 0.05	1.08
4	2 Jan	2145.46	42.407	42.82 ± 0.10	1.62
5	2 Jan	2151.10	42.673	42.90 ± 0.10	1.96
6	2 Jan	2159.10	42.785		0.50
7	2 Jan	2254.14	42.121	42.44 ± 0.10	2.17
8	2 Jan	2303.34	42.962	43.52 ± 0.10	1.65
9	2 Jan	2309.19	41.092	41.68 ± 0.10	0.67
10	2 Jan	2314.05	41.766	41.90 ± 0.10	1.00
11	2 Jan	2337.19	42.225	42.24 ± 0.05	0.96
12	3 Jan	1735.17	41.040	41.16 ± 0.05	1.25
13	3 Jan	1745.54	41.975	42.20 ± 0.10	1.75
14	3 Jan	1753.30	41.940	42.00 ± 0.10	1.20
15	3 Jan	2017.12	41.935		0.31
16	3 Jan	2316.25	42.970		0.41
17	3 Jan	2340.08	40.755		0.34
			Mean values = 42.252	42.416	

*Mean of first 6 returns.

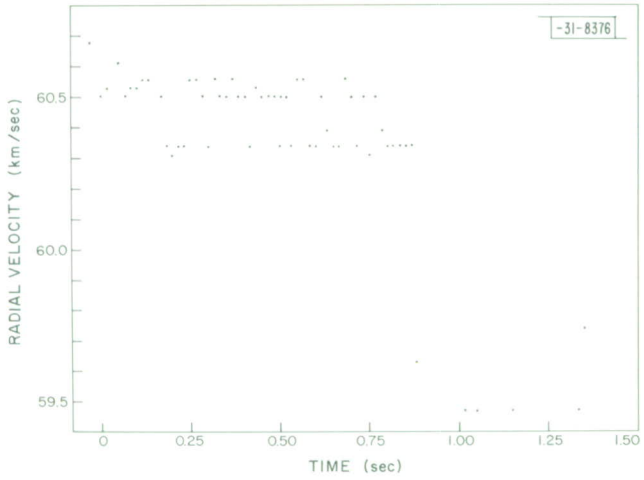

Fig. 27. Observations of radial velocity vs time for Perseid 7 (1961).

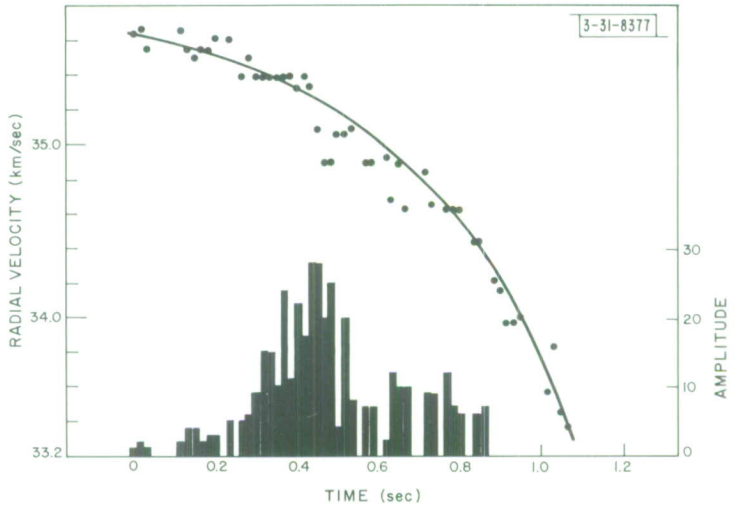

Fig. 28. Observations of radial velocity vs time for Geminid 2 (1961).

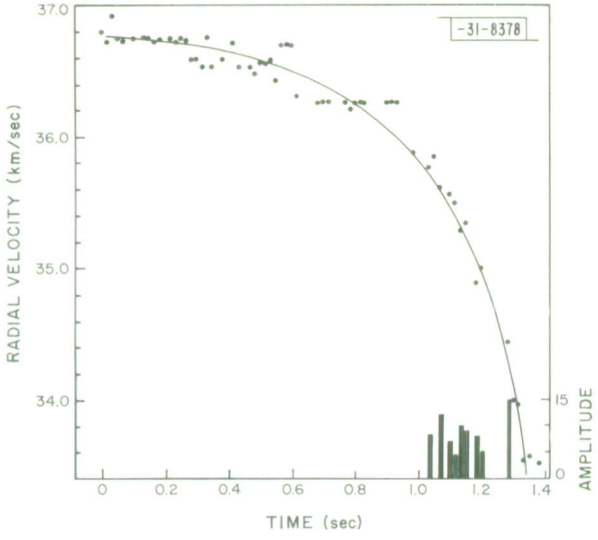

Fig. 29. Observations of radial velocity vs time for Geminid 9 (1961).

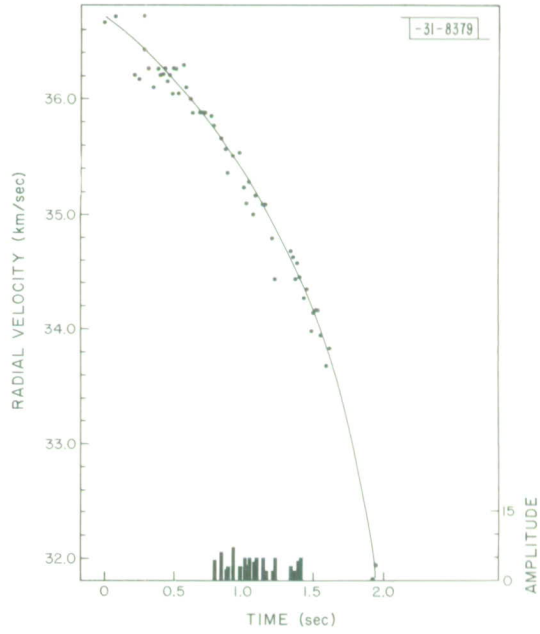

Fig. 30. Observations of radial velocity vs time for Geminid 11 (1961).

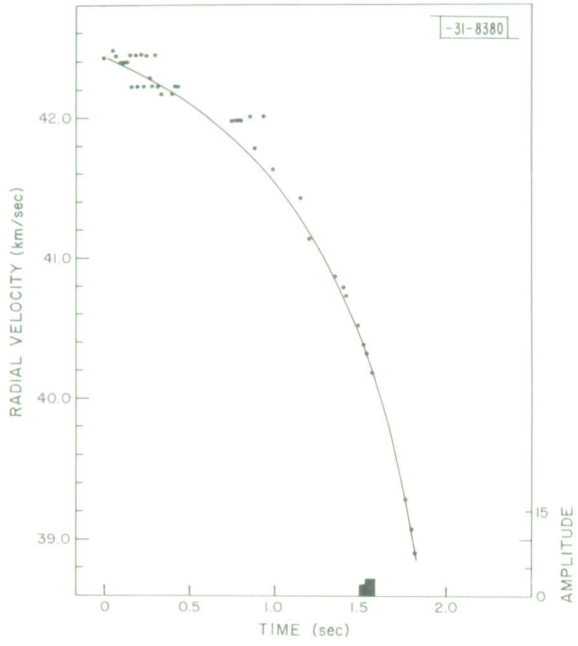

Fig. 31. Observations of radial velocity vs time for Quadrantid 5 (1962).

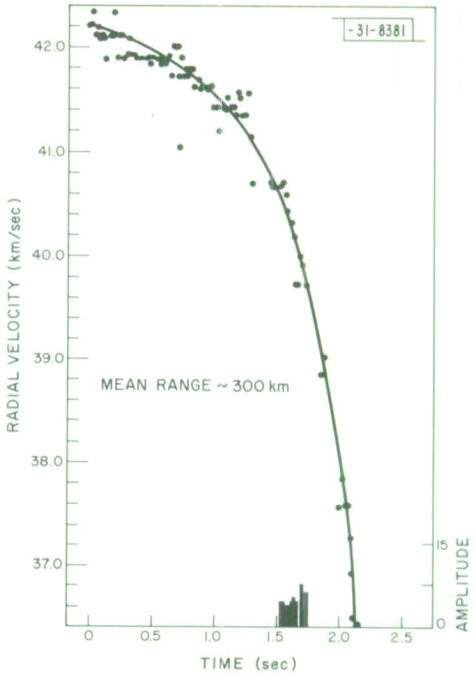

Fig. 32. Observations of radial velocity vs time for Quadrantid 8 (1962).

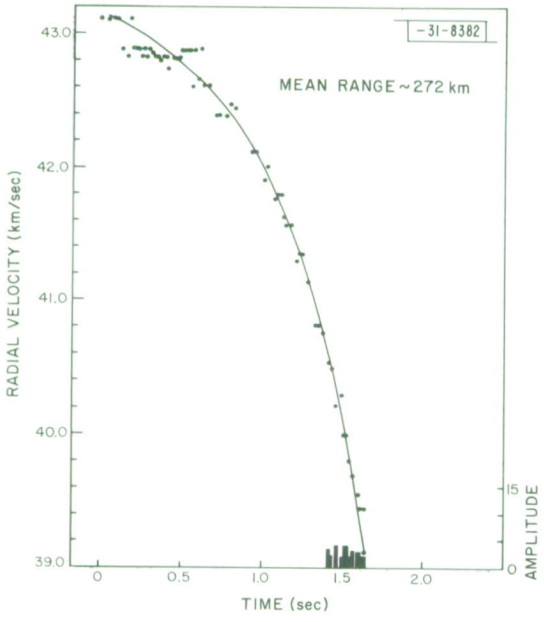

Fig. 33. Observations of radial velocity vs time for Quadrantid 9 (1962).

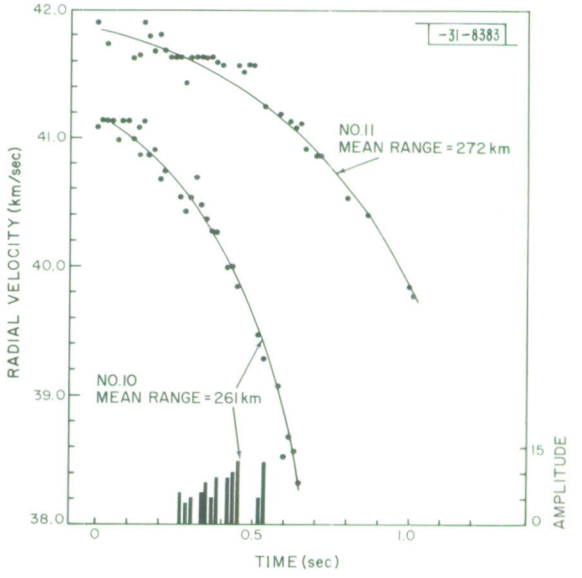

Fig. 34. Observations of radial velocity vs time for Quadrantids 10 and 11 (1962).

In photographic observations, the quantity measured is the distance traveled by the meteor as a function of time. The first derivative of this is, of course, the velocity; the second derivative is the deceleration. A reduction procedure required to determine velocity and deceleration from photographic plates has been given by Whipple and Jacchia,[13] who emphasize the care which must be taken in the process. In these radio measurements the velocity is measured directly and deceleration is the first derivative. It seems, therefore, that the values of deceleration obtainable from these plots of velocity vs time, e.g., Figs. 28 to 34, are the best presently available.

Unfortunately, even with an accurate plot of velocity vs time (such as obtained here) it is not possible to compute from theory unambiguous values for the mass of the meteor without assuming either its radius or density. This point is discussed more fully in the next section, where the theory of meteor deceleration is briefly reviewed. The principal difficulty is simply that there are too many unknowns in the equations. It is possible, however, by comparing these results with theory to estimate the effective ablation energy for unit mass and the product of the radius and density for most of the meteors. These results are presented in the next few sections.

Amplitude:– We have enumerated earlier[1] the difficulties encountered in measuring echo amplitude. Problems arise because the basic detection scheme (which employs the filter bank) is exceedingly nonlinear. For the observations of meteors traveling radially toward the radar, echo-power measurements were made with a separate IF channel having a bandwidth of 5 kcps. A larger filter would have been desirable to accommodate the wide range of doppler shifts encountered. This was not practical because the signal-to-noise ratio of most of the returns was very low and a larger filter would cause all but a few returns to be undetectable. The output from a 5-kcps-wide IF channel was connected to a detector having a logarithmic law which gave as its output a voltage proportional to the received power expressed in db. This voltage was sampled by an analog-to-digital converter on command. The command to "sample" was derived from the trigger pulse generated at the output of the filter bank on receipt of an echo. The digital word representing the echo power together with the other information pertinent to each echo (time, range, doppler, etc.) was stored in the CG 24 computer. This recording system provided a large dynamic range (better than 30 db) but unfortunately this precaution proved unnecessary as most of the returns were near the limit of detectability. In retrospect, it is evident that the alternative amplitude measuring scheme described in Ref. 1 in which a second filter bank was employed would have been more successful. The undesirable consequence of using the narrow (5-kcps) filter is that only a fraction of the amplitude data (lying within ± 2 kcps of the center frequency) can be regarded as valid. The logarithm of the power of these returns

TABLE VIII

Amplitude Value	Signal Power (dbm)	
	Geminids	Quadrantids
1	–129	–127
10	–115	–113
100	–98	–96

has been plotted on an arbitrary scale (labeled amplitude) in Figs. 28 to 34. The system was calibrated by means of a pulsed signal generator connected to the receiver via a directional coupler. The conversion of these amplitude values of signal power is shown in Table VIII. The majority of the returns lie between 5 and 10 on the amplitude scale, i.e., roughly equivalent to echo powers of between −118 and −114 dbm. Taking the mean range to be 300 km, the corresponding target cross sections lie between 10 and 25 cm^2. These cross sections are substantially lower than the average cross sections of the meteors viewed from the side, which are of the order of one to two square meters for the sporadics and larger for the Quadrantids or Geminids.

C. Theory

Contributions to the theory of the deceleration of a meteor in the earth's atmosphere have been made by a number of authors over the last 40 years. Contemporary reviews of this work have been given by McKinley,[5] Whipple and Hawkins,[7] Hawkins and Southworth,[8] Whipple,[14] and Verniani.[15] The most useful treatise on the whole subject is that by Öpik.[16] In view of this large body of literature we will not do more than outline the development of the basic equations in the remainder of the report. Unfortunately, a wide variety of different symbols for such quantities as meteor velocity, density, etc., have been used by different authors. A representative list of these symbols is given in Table IX together with the symbols which will be adopted here. In general, we have tried to follow the symbols most commonly used.

The basic physical assumptions employed in the derivation of an expression for the deceleration are as follows. It is generally assumed that the dimensions of the meteroid are small compared with the mean free path of the air molecules. At a height of 100 km the mean free path λ in air is λ = 16 cm (Ref. 17), and since most meteors probably have dimensions measured in millimeters, this assumption is almost certainly valid. At 80-km height, however, λ has become 0.40 cm (Ref. 17) and the validity of this assumption may be questioned. The air molecules impinging on the surface of the meteor do so individually and no air cap will be formed, provided that the mean free path is much larger than the size of the meteoroid. If the mean free path becomes comparable with the dimensions of the meteoroid then air molecules that have collided with the advancing meteor cannot escape freely. Instead, they suffer a collision with other air molecules before they have traveled far from the meteor. Thus, air becomes trapped in front of the meteoroid cutting down the rate of heating of the meteor. It seems probable that cap formation commences in the middle of the meteor region. This complication is ignored in many reviews and of those listed, only Öpik[16] has treated the problem in detail. From the values for the height (to be presented in Table XI), it seems safe to assume that the formation of an air cap would be unlikely for many of the meteors reported here.

The next assumption that is widely made concerns the mechanics of the impact of the air molecules. It seems probable that most of the air molecules are occluded onto the surface of the meteor and liberated a short time later. Most theories simply assume that the collisions are largely inelastic and, that on the average, the angle through which the air molecule will be scattered is that of specular reflection. During one second the meteor will encounter a total air mass of $\sigma\rho v$ where σ is the physical cross section of the meteor, ρ is the air density, and v the meteor velocity. If all the collisions were central and elastic then the total kinetic energy given to the air would be $\sigma\rho v^3$ and no heating of the meteor would occur. Because it is widely

TABLE IX

SYMBOLS

This Paper	Öpik*	Whipple and Hawkins†	Verniani‡	Explanation
m	M	m	M	Meteor mass (function of time)
v	ω	v	v	Meteor velocity (function of time)
v_∞			v_o	Initial speed of the meteor
δ	δ	ρ_m	ρ	Density of a meteoroid
ρ	ρ	ρ	ρ_a	Atmospheric density
σ	σ	s	σ	Meteor cross section
		A	A	Dimensionless shape factor
γ	ξ_K	Γ	γ	Drag coefficient
χ	z	z	χ	Zenith angle
H	a	H	H	Atmospheric scale height
h	H	h	z	Height or altitude
ℓ	h	ξ	ℓ	Heat of ablation
Λ	γ	Λ	Λ	Heat transfer coefficient
r	r		r	Equivalent radius of the meteor
λ	λ_o			Mean free path in air
ξ			ξ	Effective ablation energy = $\gamma\ell/\Lambda$

* See Ref. 16.

† See Ref. 14.

‡ See Ref. 15.

thought that the collisions are mostly inelastic, an amount of kinetic energy $1/2\,\sigma\rho v^3$ is given up each second, and some fraction Λ of this goes toward heating the meteor. The quantity Λ is called the heat transfer coefficient and is the net coefficient of transfer, i.e., the difference between the kinetic transfer and the loss through radiation and sputtering.

The heat given to the meteoroid is initially distributed only over the surface. This heat will chiefly be expended in vaporizing the surface layers and not in heating the meteor as a whole if the thermal conductivity is low. If ℓ is the heat of ablation (the heat required to ablate one gram of the material), then from conservation of energy it follows that

$$\ell \frac{dm}{dt} = -\frac{1}{2} \Lambda \sigma \rho v^3 \quad , \tag{12}$$

where dm/dt is the rate of loss of mass by the meteor. The velocity v is, of course, not constant. However, since $v \propto (dm/dt)^{1/3}$, v may be taken as constant until a very large fraction of the meteor mass has been ablated. Equation (12) is generally known as the mass equation.

A second equation of importance can be obtained by considering conservation of momentum. The momentum given in unit time to the air molecules in completely inelastic collisions would be the air mass ($\rho\sigma v$) times the velocity (v) i.e., $\rho\sigma v^2$. However, the final velocity of the air molecules may be somewhat less than v and hence the meteor momentum destroyed per unit time can be written as $\gamma\rho\sigma v^2$, where γ is a dimensionless drag coefficient. Hence, we have

$$m \frac{dv}{dt} = -\gamma \rho \sigma v^2 \quad . \tag{13}$$

This is the drag equation. In a time dt the meteor will travel a linear distance $v \sec\chi\, dh$, where χ is the angle between the meteor path and the zenith. It follows that (13) can be written

$$\frac{dv}{dh} = -\frac{v\gamma\rho\sigma \sec\chi}{m} \quad . \tag{14}$$

The observations of the deceleration of the meteors presented in the previous section provide v, dv/dh, and $\sec\chi$ as functions of time. Thus, provided that γ can be estimated from theory, the variation of $\sigma\rho/m$ as a function of time can be obtained.

By combining the drag and the mass equations one obtains

$$\frac{1}{2\xi} v\, dv = \frac{dm}{m} \quad , \tag{15}$$

where $\xi = \gamma\ell/\Lambda$ is the effective ablation energy for unit mass and has a value $\sim 16\,km^2 s^{-2}$, according to Verniani.[18] The observations described here permit this value to be tested. By integrating (15) one obtains

$$m = m_\infty \exp\left[\frac{v^2 - v_\infty^2}{4\xi}\right] \quad , \tag{16}$$

where v_∞ and m_∞ are the initial velocity and mass of the meteor, respectively. Introducing an equivalent radius for the meteor Eq. (16) becomes

$$r = r_\infty \exp\left[\frac{v^2 - v_\infty^2}{12\xi}\right] \quad . \tag{17}$$

We shall not continue the development of all the various possible equations, but simply present some of the more important ones in Table X. These have been taken from the paper by Verniani.[15]

TABLE X

VARIATIONS OF EQUATION 16

$$q = \frac{9}{4} q_{max} \frac{\rho}{\rho_{max}} \left(1 - \frac{\rho}{3\rho_{max}}\right)^2 \tag{18}$$

$$v = v_\infty \left[1 + \frac{12\xi}{v_\infty^2} \ln\left(1 - \frac{\rho}{3\rho_{max}}\right)\right]^{1/2} \tag{19}$$

$$a = \frac{2}{3} a_{max} \frac{\rho}{\rho_{max}} \left(1 - \frac{\rho}{3\rho_{max}}\right)^{-1} \tag{20}$$

$$r = r_\infty \left(1 - \frac{\rho}{3\rho_{max}}\right) \tag{21}$$

$$m = m_\infty \left(1 - \frac{\rho}{3\rho_{max}}\right)^3 \tag{22}$$

$$r_{max} = \frac{2}{3} r_\infty \tag{23}$$

$$m_{max} = \frac{8}{27} r_\infty \tag{24}$$

$$v_{max} = v_\infty - \frac{12\xi}{5v_\infty} \tag{25}$$

$$a_{max} = \frac{3\xi}{H} \cos\chi \tag{26}$$

The subscript max denotes the value of the preceding quantity at the point where the ablation rate is a maximum; the symbol ∞ denotes the initial value, i.e., before entering the earth's atmosphere.

The subscript max denotes the value of the quantity when the ablation rate is at its maximum. The quantities employed are:

q = line density

ρ = atmospheric density

v = meteor velocity

$\xi = \gamma\ell/\Lambda$ = effective ablation energy

a = modulus of the meteor deceleration

r = equivalent radius of the meteor

m = meteor mass

H = atmospheric scale height

χ = zenith angle of the path.

These equations are only approximately correct and Verniani[15] states that an exact value for the velocity must be obtained by solving

$$\rho = \frac{2}{3}\frac{\delta g r_\infty}{\gamma F}\cos\chi \exp\left[\frac{-v_\infty^2}{12\xi}\right]\left[E\left(\frac{v_\infty^2}{12\xi}\right) - E\left(\frac{v^2}{12\xi}\right)\right] \quad , \tag{27}$$

where δ = density of the meteoroid, g = acceleration due to gravity, $E(\chi)$ indicates the logarithmic integral, and F is a shape factor employed by Verniani defined in

$$\sigma = F\pi r^2 \quad . \tag{28}$$

The difference between the solution of (27) for a meteor with initial velocity v_∞ = 40 km/sec and Eq. (19) is illustrated in Fig. 35; the difference in the behavior of the equivalent radius r for the two solutions is illustrated in Fig. 36. (These figures have been taken from Ref. 15.)

D. Comparison with Theory

The results for the velocity of the approaching meteors (Figs. 28 to 34), provide velocity as a function of time with respect to the commencement of the event. Curves were plotted for all the meteors with durations greater than about 0.75 second. Values for the initial velocity v_∞ were estimated from these curves and have been presented in Tables VI and VII.

Tables of values of the velocity as a function of height were next computed in the following manner. The smooth curves for velocity vs time were read off at 0.05-second intervals to provide tables of velocity vs time. The height of the first point in this table was computed using the mean of all the values for the range in the 0.1-second interval centered on this time, by assuming that the meteor lies on the axis of the beam. Due to the finite width of the beam this assumption probably introduces an error of no more than ±2 percent of the range. The range values lie between about 200 and 400 km and hence there is an uncertainty in the absolute height of as much as ±1 scale height (7 km). This is unfortunate and in principle could have been overcome by employing a split-beam technique. It was not possible to use this procedure at the time.

The values for the height at subsequent times were computed by assuming that the meteor continues to travel toward the radar along the axis of the beam, and that it travels a linear distance of $0.05\bar{v}$ km in each 0.05-second interval (where $\bar{v}$ is the mean of the velocities at the beginning and end of this interval). The tables of velocity vs height constructed in this manner are included in the Appendix.

The aforementioned tables provide a smooth variation of velocity vs height and do not reflect the large errors in the individual range measurements. The absolute height of the whole meteor is, however, uncertain by as much as 1 scale height. Errors in the velocity curve due to the meteor intersecting the antenna beam at a small angle cannot, of course, be corrected.

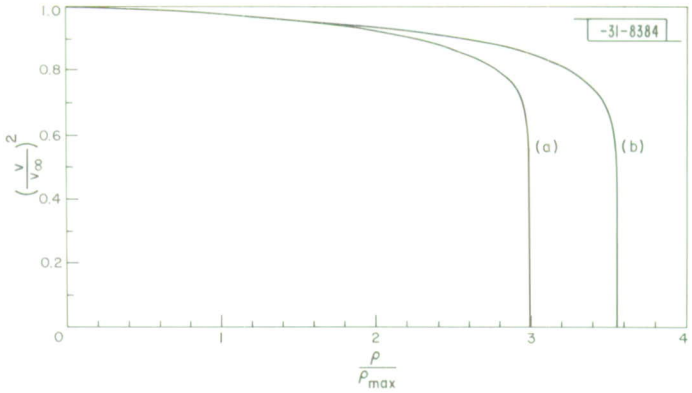

Fig. 35. Theoretical variation of velocity of a meteor with initial velocity 40 km/sec as a function of atmospheric density ρ normalized to density ρ_{max} at point of maximum ablation rate. (a) The approximate solution [Eq. (19)]. (b) The full solution for velocity [Eq. (27)], after Verniani.[15]

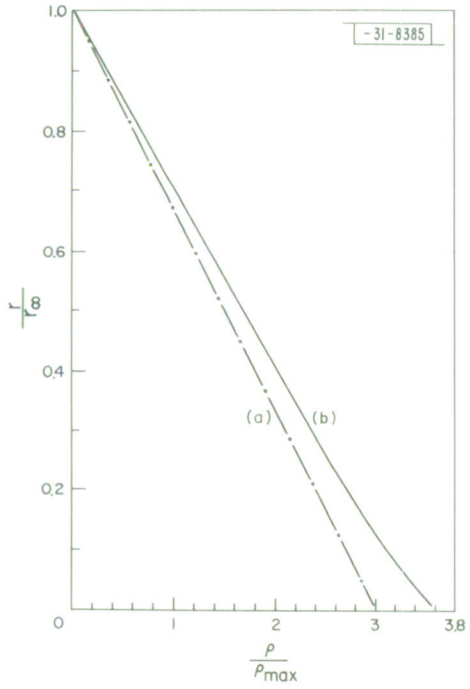

Fig. 36. Theoretical variation of equivalent meteor radius r as a function of atmospheric density ρ. (a) The approximate solution given in Eq. (21). (b) The more rigorous solution (Verniani[15]).

Attempts have been made to compare the observed deceleration with that predicted theoretically, assuming free molecular flow (no air cap). Curves of v/v_∞ were prepared for different values of the effective ablation energy ξ (equal to 6, 10, 14, 18, and 22 km^2/sec^2) for both the Geminids and Quadrantids (v_∞ equal to 36.0 and 42.5 km/sec, respectively), using the approximate expression [Eq. (19)]. These curves were plotted on a height scale marked off in kilometers, with respect to the height h_{max} at which the maximum rate of ablation occurs. Because we have no way of determining h_{max} from our observations, the observed velocity ratios v/v_∞ were plotted against an arbitrary height scale and the two graphs were then adjusted for best alignment between the observed and any one of the theoretical curves. In practice it was also necessary to adjust the graphs vertically to correct for errors in the estimated value of v_∞. It is easy to show that the first-order effect of a small error Δv in estimating the true value of v_∞ alters all the values of v/v_∞ by the same amount ($\Delta v/v_\infty$). Hence, the true value of v_∞ together with ξ and h_{max} can be obtained by this fitting procedure. The results of this work are summarized in Table XI. In many cases the duration of the meteor was insufficient to distinguish between different theoretical curves. An example of this is provided in Fig. 37 where Quadrantid 13 can be seen to fit the curves for $\xi = 14$ and $\xi = 18\ km^2/sec^2$. In these cases both solutions have been given in Table XI. In a small number of cases only one solution seemed possible – Geminid 8, for example (Fig. 38). For a very large number, no proper fit could be obtained to any of the curves because the deceleration was not sufficiently rapid toward the end of the event. Examples of this behavior are shown in Figs. 38 and 39 by Geminid 11 and Quadrantids 5 and 8. In two cases this could be attributed to the use of the approximate solution for the velocity [Eq. (19)] in place of the more rigorous one [Eq. (27)]. The difference in predicted behavior for these two solutions is illustrated in Fig. 37, for $\xi = 10$, and seems sufficient to explain why Quadrantids 6 (Fig. 39) and 14 do not fit the theoretical curve. However, in the other cases (Geminid 11, Quadrantids 5, 8, and 9), the departure between theory and experiment is too marked to be explained by the use of the approximate theory and suggests that, in fact, an air cap forms around the meteor. This process reduces γ (the drag coefficient), and consequently reduces ξ (equal to $\gamma\ell/\Lambda$), the effective ablation energy. Thus, a meteor which begins by following a particular curve for ξ (e.g., Geminid 11 follows $\xi = 18$) will gradually depart from this line toward curves of lower values of ξ.

By noting the height at which this effect occurs, we can roughly estimate the height when cap formation commences. A mean of the observed heights is 99 km, but this is an overestimation because the observations would probably fit curves for the exact solution down to somewhat lower heights (perhaps 98 km).

A mean for all the values of ξ listed in Table XI is $\xi = 15.4\ km^2/sec^2$ – a value in remarkable agreement with that employed by Verniani[18] ($\xi = 16\ km^2/sec^2$) in his reduction of photographic data published by Whipple.[19] The spread of values is large and suggests that individual meteors may behave with values widely different from this average value. There is no clear cut difference between the Geminids and Quadrantids in Table XI, and we cannot comment on Jacchia's result that ξ increases with velocity.[20]

E. Meteor Masses

In Eq. (14) we developed an expression containing the meteor mass m and cross section

$$\frac{dv}{dh} = -\frac{v\gamma\rho\sigma \sec\chi}{m} \quad . \tag{14}$$

TABLE XI

DOWN-THE-BEAM METEORS

Event		Estimated v_∞	1st Solution ξ	1st Solution v_∞	1st Solution h_{max}	2nd Solution ξ	2nd Solution v_∞	2nd Solution h_{max}	Comments	Assumed v_{max}	Mean $r\delta$	Mean Height	Mean $\cos \chi$
Geminid	2	35.7 ± 0.05	14	35.89	94.8	18	35.92	93.2	Fits both solutions equally	34.76	0.088	96.48	0.3368
	4	36.6 ± 0.2	18	36.42	91.6	22	36.47	90.75	Fits both solutions equally	34.98	0.123	92.66	0.3353
	6	36.72 ± 0.05	(Appears to have fragmented)						Fits no solution		0.784	89.10	0.1683
	9	36.80 ± 0.05	8	36.92	101.0				Fits this value only*	36.33	0.064	101.35	0.2876
	11	37.2 ± 0.2	18	37.20	95.4				Poor fit below 96 km*	35.86	0.127	93.65	0.1969
	13	37.0 ± 0.05	18	37.18	96.95	14	37.15	98.0	Fits both solutions equally	35.98	0.054	101.03	0.2974
Mean value		36.55†	Mean of all solutions v_∞ = 36.73							35.58	0.207	95.7	
Quadrantid	1	42.9 ± 0.2	10	42.60	101.65				Fits this value only	42.00	0.056	102.13	0.2687
	2	42.64 ± 0.05	6	42.79	106.3	10	42.79	103.8	Fits these and other solutions	42.31	0.059	106.33	0.2015
	4	43.32 ± 0.1	6	43.47	85.75	10	43.47	83.2	Fits these and other solutions	42.97	3.836	86.00	0.1723
	5	42.82 ± 0.1	10	42.63	99.0	14	42.69	97.85	Poor fit below 99 km*	41.93	0.138	96.48	0.1882
	6	42.9 ± 0.1	18	43.00	101.5				Poor fit below 78 km*	41.90	0.055	102.27	0.1942
	8	42.44 ± 0.1	22	42.44	98.8				Poor fit below 106 km*	41.11	0.078	99.25	0.2266
	9	43.52 ± 0.1	22	43.41	93.75	18	43.41	94.75	Poor fit below 96 km	42.17	0.172	94.40	0.2324
	10	41.68 ± 0.1	18	42.03	94.8				Fits this value only	40.95	0.120	92.78	0.2365
	11	41.90 ± 0.1	18	42.21	101.9	14	42.13	102.8	Fits both solutions equally	41.21	0.035	102.85	0.2468
	12	42.24 ± 0.05	14	42.45	105.0	18	42.55	104.2	Lies between these values	41.53	0.027	105.78	0.2409
	13	41.16 ± 0.05	14	41.34	103.25	18	41.36	102.1	Fits ξ = 18 better*	40.41	0.039	104.83	0.2311
	14	42.20 ± 0.1	18	42.12	109.85	22	42.16	109.2	Poor fit below 112 km	40.94	0.011	111.88	0.2279
Mean value		42.42†	Mean of all solutions v_∞ = 42.46							41.62	0.385	100.4	

* Values plotted (Figs. 37 to 39).

† Values obtained from Tables VI and VII.

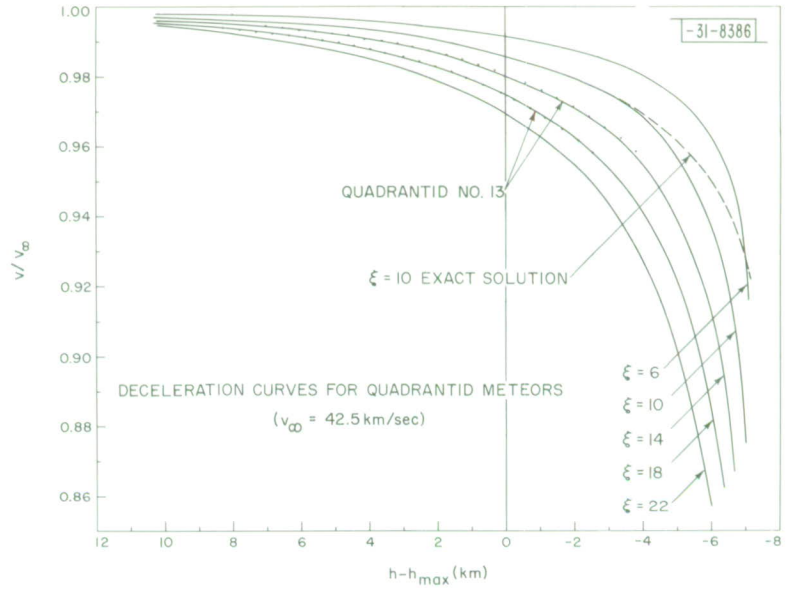

Fig. 37. Variation of velocity observed for Quadrantid 13 superimposed on theoretical curves for different values of ablation energy ξ. (It can be seen that this event was of insufficient duration to define ξ precisely.)

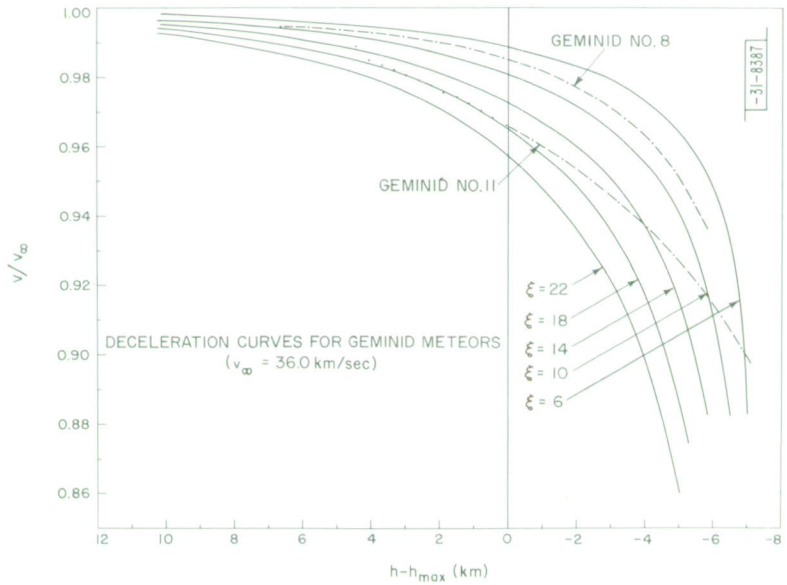

Fig. 38. Variation of velocity for Geminids 8 and 11. In the case of 8 it is believed that $\xi = 8$ represents the only likely solution. Geminid 11 departs by an amount interpreted as being caused by formation of an air cap.

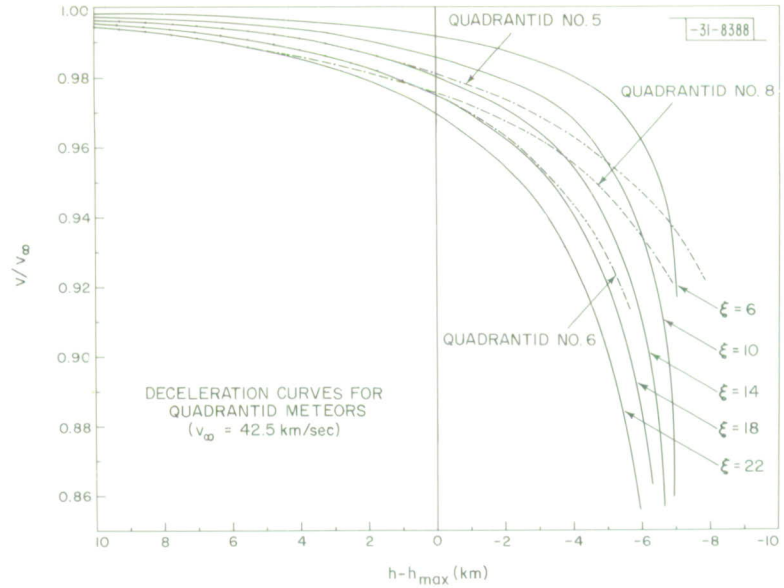

Fig. 39. Variation of velocity for Quadrantids 5, 6 and 8. Event 6 departs from the theoretical curve by an amount which can be attributed to the fact that approximate solutions (see Fig. 37) have been employed. Both events 5 and 8 depart from theoretical curves in a manner which indicates that an air cap has been formed.

The mass m depends upon both the size and density of the meteor; whereas, the cross section σ depends upon the shape and the size. One of these variables can be removed if assumptions are made concerning the shape of the meteor. Thus, Öpik[16] introduces the equivalent radius r defined in

$$m = \frac{4}{3}\pi r^3 \delta \quad , \tag{29}$$

where δ = meteor density, as a measure of the size. The cross section may then be expressed as

$$\sigma = 4J\pi r^2 \quad , \tag{30}$$

where J is a shape factor which would have a value of 0.25 if the particle were in fact a sphere. For an average solid meteoroid of not too unusual shape, Öpik adopts a value

$$J = 0.5 \pm 0.1 \quad . \tag{31}$$

We also need to know the drag coefficient γ in Eq. (14). Öpik[16] adopts a value of unity for small meteors in which no air cap is formed. Thus, the product $\gamma\sigma$ becomes

$$\gamma\sigma = 2\pi r^2 = 6.28\, r^2 \quad . \tag{32}$$

We have adopted this value in the calculations which follow. We note, however, that different assumptions have been made by Whipple and Hawkins,[7] Hawkins and Southworth,[8] and McKinley,[5] who has followed the formulation of Whipple and Hawkins. In this treatment the cross section of a sphere is written as

$$\sigma = \left(\frac{9\pi}{16}\right)^{1/3} \delta^{-2/3}\, m^{2/3} \quad , \tag{33}$$

thereby removing the equivalent radius r as one of the parameters. Any object other than a sphere has a cross section which may be written

$$\sigma = A\delta^{-2/3} m^{2/3} \quad , \tag{34}$$

where A is a dimensionless shape factor having a value $(9\pi/16)^{1/3}$ (equal to 1.2) for a sphere. For a cube entering the atmosphere face on, A = 1.0; for a cube with one edge leading, A = 1.4. When a cube moves with one corner leading, A = 2.5. Thus, there is a very approximate relationship between the shape factor J used by Öpik and A, namely, $J \sim A/4$.

The drag coefficient γ will have a value of 1.0 for free molecular flow, but will be reduced to about 0.4 when an air cap is formed. Whipple and Hawkins[7] therefore favor values of $A > 1$ and $\gamma < 1$ and are inclined to believe (on the basis of available information) that the value of γA may be taken as unity. (Earlier, Jacchia[21] employed a value for the product $\gamma A\delta^{-2/3}$ equal to 1.0.) Thus, from (34) we have for the product of the drag coefficient and the cross section according to Whipple and Hawkins[7]

$$\gamma\sigma = \delta^{-2/3} m^{2/3} \quad . \tag{35}$$

When expressed in terms of Öpik's equivalent radius r (35) yields

$$\gamma\sigma = \left(\frac{4\pi}{3}\right)^{2/3} r^2 = 2.6\, r^2 \quad . \tag{36}$$

Yet a third approach has been adopted by Verniani[15] in which the cross section is written as

$$\sigma = F\pi r^2 \quad , \tag{28}$$

where F is another shape factor and has the value F = 1 for a sphere. In handling the reduction of a large number of meteors, Verniani assumes that the average value of F is unity and proceeds to compute values for the mean drag coefficient $\bar{\gamma}$. The values obtained in this manner seem to increase linearly with height (implying cap formation) and an appropriate value for h equal to 100 km would be $\gamma = 0.80$. Thus, at this height, the value adopted by Verniani for the product of the cross section and drag coefficient might be

$$\gamma\sigma = 0.8\,\pi r^2 = 2.51\, r^2 \quad , \tag{37}$$

which is comparable to that employed by Whipple and Hawkins[7] [Eq. (36)]. We see then that Öpik's value for $\gamma\sigma$ is ~2.4 times that suggested by Whipple and Hawkins[7] or Verniani.

Combining Eqs. (14), (29), and (32) we obtain (following Öpik)

$$\frac{dv}{dh} = \frac{3}{2}\,\frac{1}{\delta}\left(\frac{v\rho \sec\chi}{r}\right)_h \quad , \tag{38}$$

in which all the quantities in parenthesis are functions of height. It follows that since dv/dh, ρ, $\sec\chi$, and v are known we may obtain $r\delta$ as a function of height. Had we chosen to follow Whipple and Hawkins,[7] the values of $r\delta$ would be uniformly reduced by 2.4.

Values of $r\delta$ were obtained for each of the velocity values (at 0.5-sec intervals) listed in the Appendix. This was performed in the following way. The values of dv/dh required in (38) were first obtained from the difference between adjacent values of velocity and height in the tables presented in the Appendix.

A better approach might have been to perform a least-mean-square fit, but the accuracy achieved using simple differences seemed adequate for the present purpose. Next, the atmospheric density ρ was found (from the U. S. Standard Atmosphere)[17] by making a table of density and scale height at 2-km intervals above 70 km. Interpolation using the appropriate scale height was then employed to obtain the density at any given height. The remaining term ($\sec\chi$) was obtained from the range R (computed at the time the height h was computed), together with the value of the antenna elevation angle α from

$$\cos\chi = \frac{R + R_E \sin\alpha}{(R_E^2 + R^2 + 2RR_E \sin\alpha)^{1/2}} \quad , \tag{39}$$

in which R_E is the radius of the earth.

We now form a table in which the corresponding values of v, dv/dh, h, $\sec\chi$, and ρ are known. Hence, the product of meteor radius and density $r\delta$ can be computed from (38). These values are tabulated in the Appendix.

We should expect that if the meteor atoms are ablated singly the density δ would remain constant. Then the variation of $r\delta$ with density should follow the curve given in Fig. 36. We have checked to see whether this is so. By taking the values of h_{max} given in Table XI (or a mean where two values are given) we can determine the value of the atmospheric density ρ_{max} at the point of maximum ablation. We do not know the initial radius of the meteor r_∞ and, hence, we make use of the fact that $r_{max} = 2/3\ r_\infty$ [Eq. (23)]. Thus, each value of $r\delta$ in the Appendix was divided by the corresponding value $r\delta_{max}$ obtained by interpolation, i.e., the value of $r\delta$ at h_{max}. These ratios were plotted as a function of ρ/ρ_{max}. The points are forced to pass through the expected value at $\rho = \rho_{max}$ by multiplying each ratio r/r_{max} by 2/3. The results of these operations are given in Figs. 40(a-q); the theoretical variation is also shown.

Upon inspecting these results we find that in some cases (Quadrantids 10, 11, 12, and 13), there is fair agreement between theory and experiment. However, in many cases (Geminids 2, 4, and 11 and Quadrantids 1, 5, 8, and 9), there is violent disagreement. These cases are largely those which were recognized in the previous section as being events in which an air cap formed. However, the plots of r/r_∞ provide a more sensitive test of cap formation. We note that in six cases (Geminids 4 and 13, and Quadrantids 1, 5, 8, and 9), where the departure of theory and observation seems to exist from the very commencement of the event, the mean height at which these events were first observed is 104 km.

Despite the differences between theory and experiment, the mean values of $r\delta$ do have some significance. They have been plotted as a function of height in Fig. 41 and are listed for each meteor in Table XI. It can be seen (Fig. 41) that the values are distributed in height with a similar variation to the air density – an effect that can in part be explained by the large uncertainty in the true height of the meteor (± 7 km). This effect alone would distribute the values over one order of magnitude, but since the values are distributed over two orders of magnitude, we are forced to conclude that there is an order-of-magnitude variation in radius (assuming the densities are similar). This would lead to marked differences in behavior. We can arrive at crude estimates of the average mass and radius by assuming a value for δ the density. The mean values of $r\delta$ (Table XI) are biased by two very large values (Geminid 6, which appears to have fragmented and given an erroneous value, and Quadrantid 4). Eliminating these and Quadrantid 14 which is particularly low the mean value of $r\delta$ is ~ 0.08 gm/cm^2. Assuming $\delta \sim 1$ gm/cm^3 then the average radius ~ 0.08 cm and with considerably more uncertainty the average mass $\sim 10^{-2} - 10^{-3}$ gm.

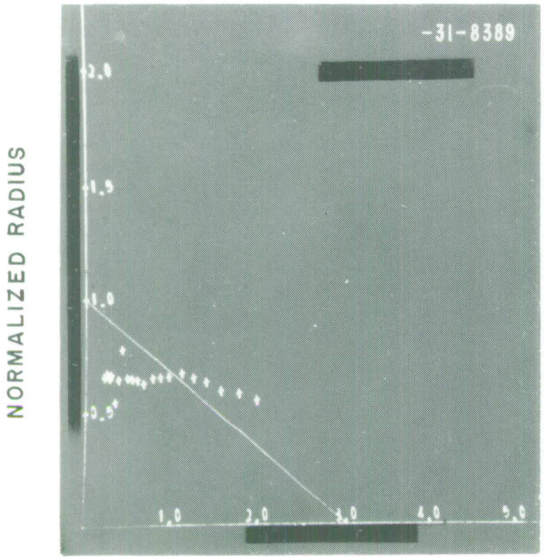

(a) Geminid 2.

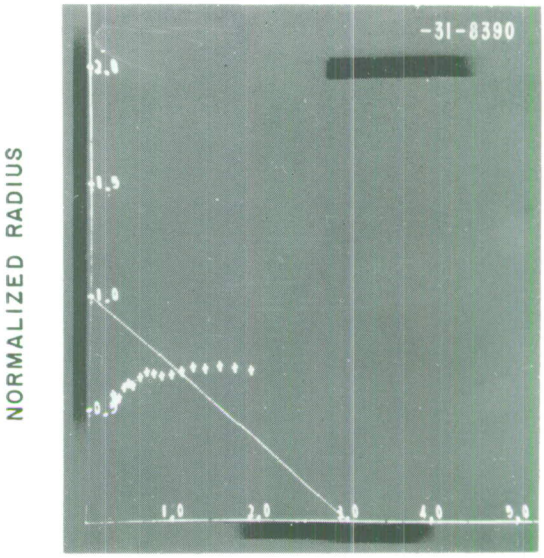

(b) Geminid 4.

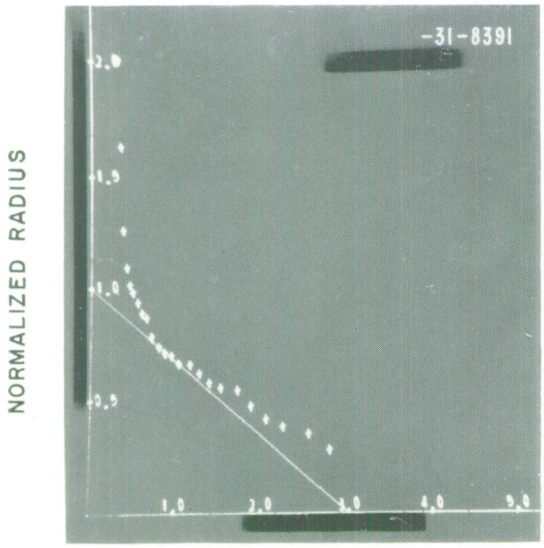

(c) Geminid 9.

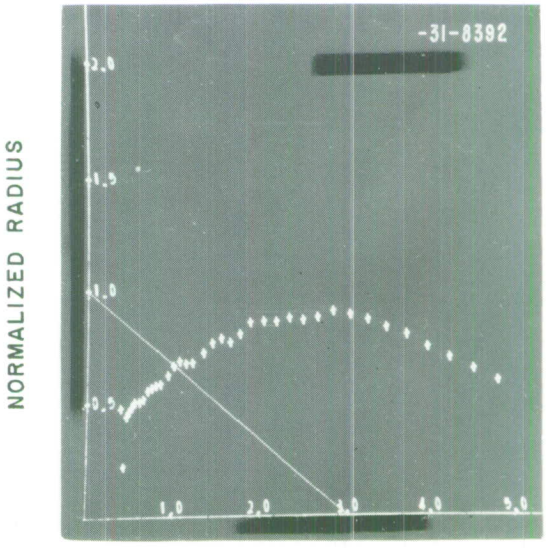

(d) Geminid 11.

Fig. 40. Observed and predicted variation of meteor radius plotted as a function of atmospheric density.

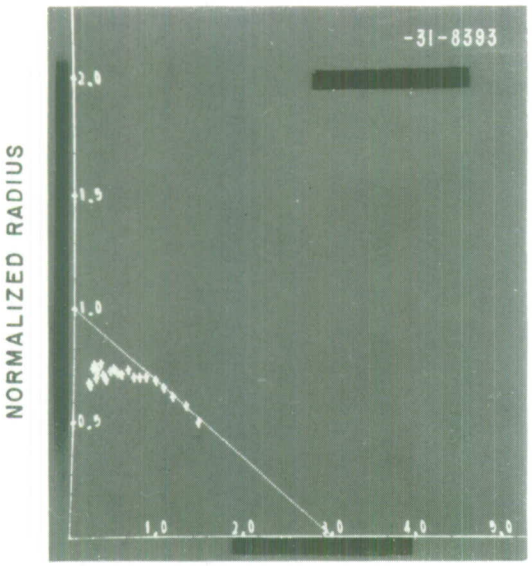

(e) Geminid 13.

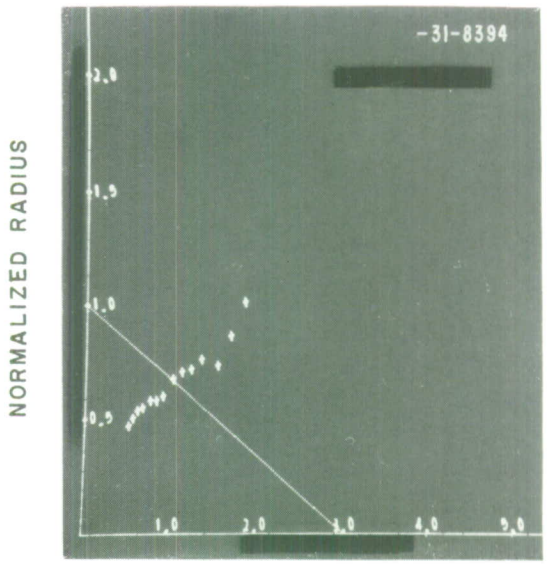

(f) Quadrantid 1.

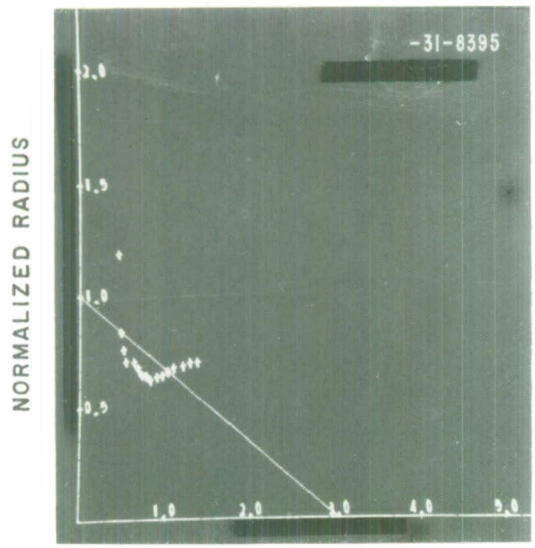

(g) Quadrantid 2.

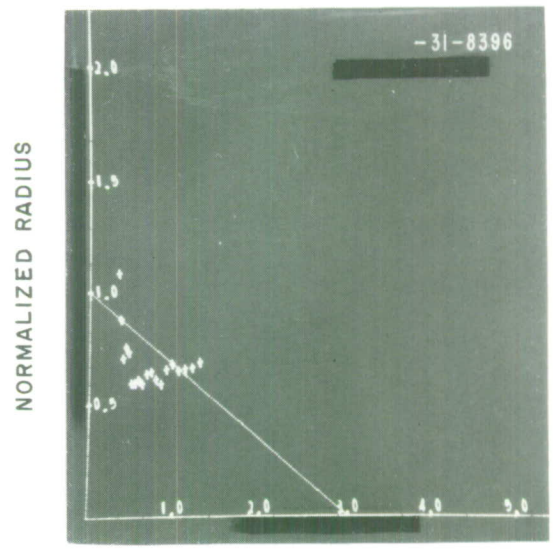

(h) Quadrantid 4.

Fig. 40. Continued.

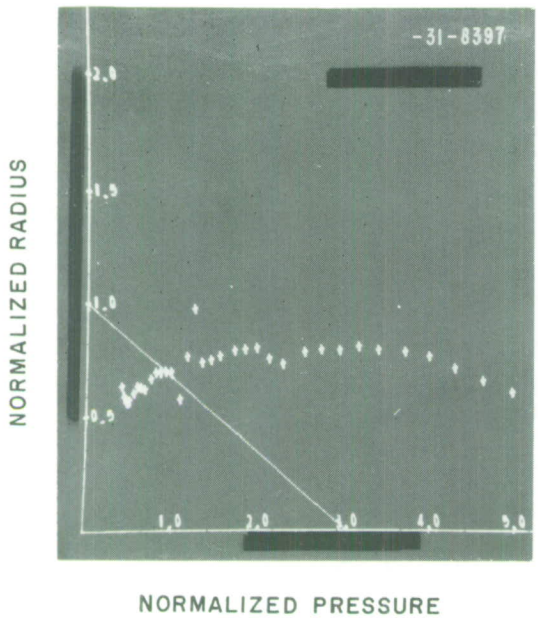

(i) Quadrantid 5.

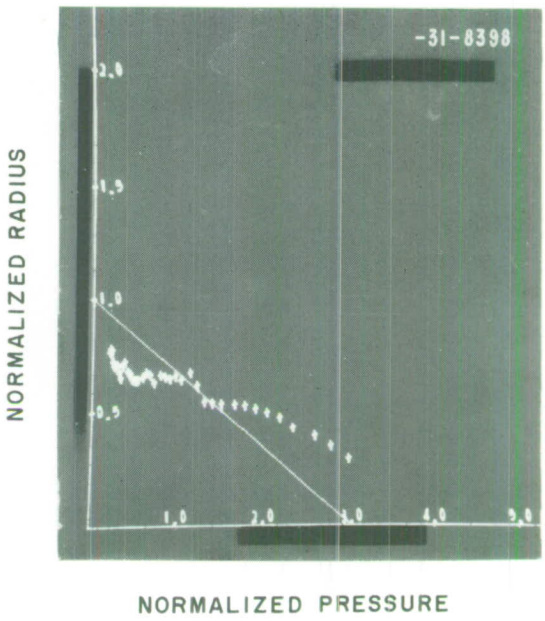

(j) Quadrantid 6.

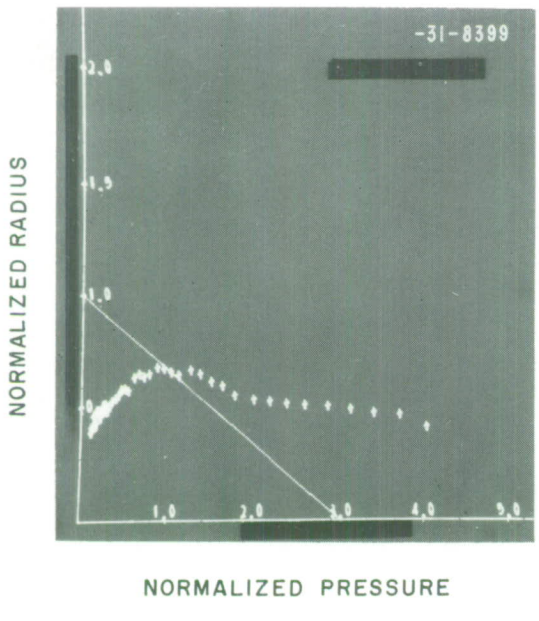

(k) Quadrantid 8.

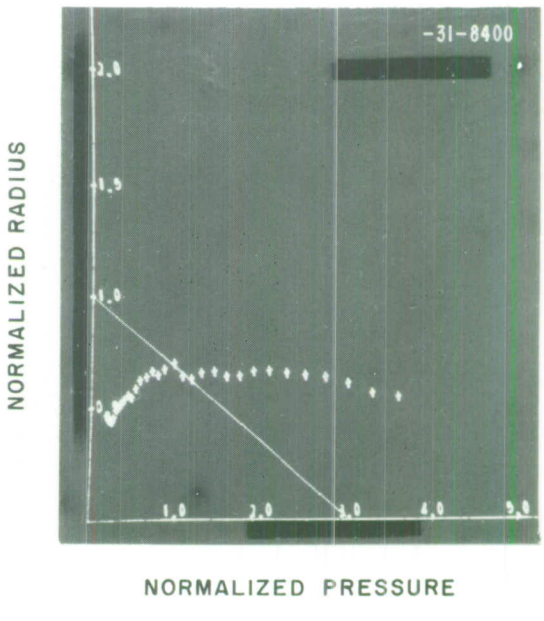

(l) Quadrantid 9.

Fig. 40. Continued.

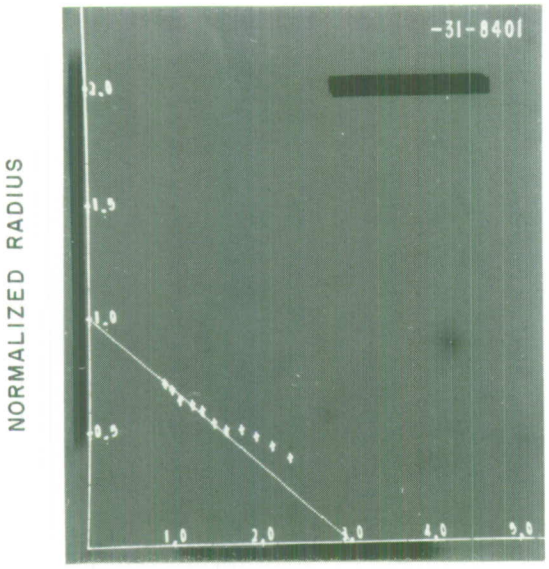

(m) Quadrantid 10.

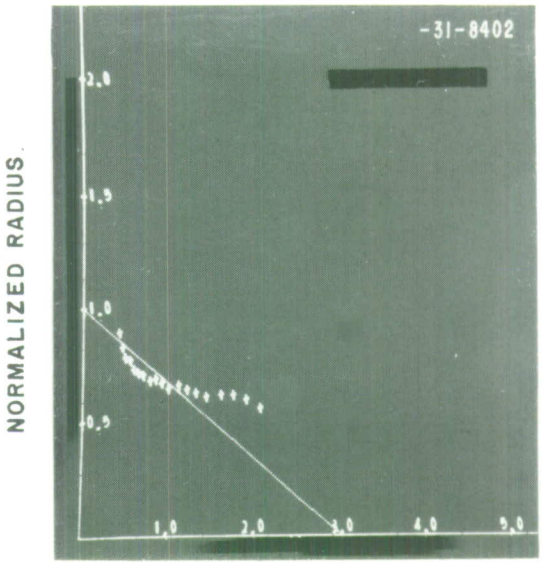

(n) Quadrantid 11.

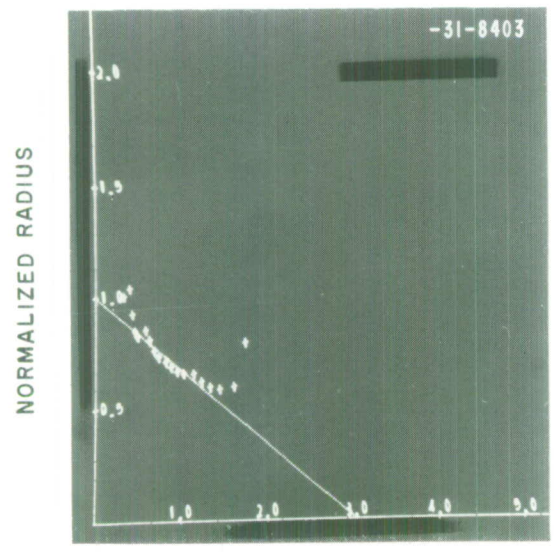

(o) Quadrantid 12.

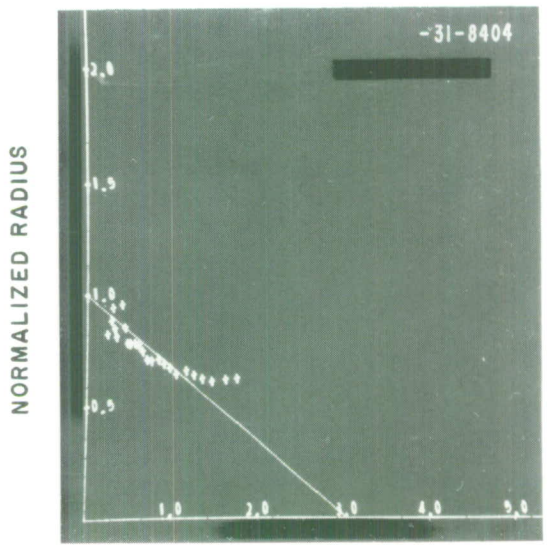

(p) Quadrantid 13.

Fig. 40. Continued.

(q) Quadrantid 14.

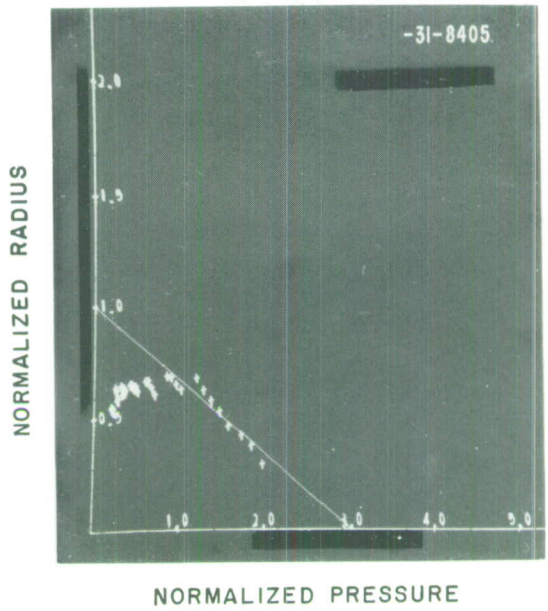

Fig. 40. Continued.

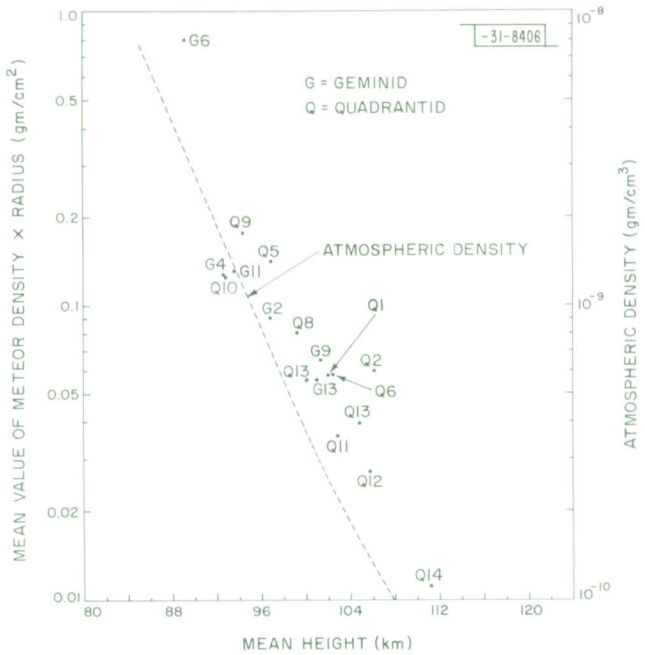

Fig. 41. Mean values of the product of radius and density of the meteors plotted as a function of the mean height of each event. The values show a range of two orders of magnitude; some of this spread must be attributed to errors in the determination of height.

Since the radius was observed to vary by at least an order of magnitude the masses must vary over three orders of magnitude.

F. Drag Coefficient γ

In Fig. 40 the points shown do not always form a smooth curve. This is probably caused in part by errors introduced by the way in which the quantity dv/dh was obtained. There is also a tendency for the curve to depart from theory at the beginning and end, which perhaps indicates error in the way in which the smooth curve was drawn through the original velocity vs time points.

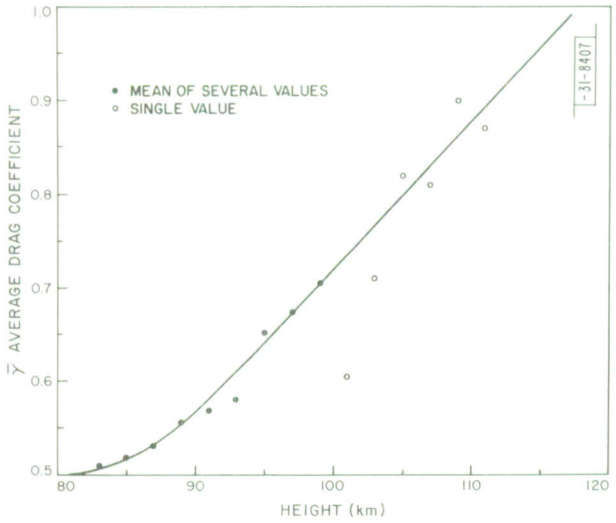

Fig. 42. Mean values of drag coefficient $\bar{\gamma}$ obtained by Verniani[18] (by analyzing photographic data) averaged and plotted as a function of height. Results are few and uncertain above 100 km but indicate that an air cap commonly forms around photographic meteors above such heights. Similar behavior seems evident in radio observations reported here.

We attribute other major departures to one of two physical effects – fragmentation or cap formation. One meteor (Geminid 6) suffered a very rapid deceleration which can only be attributed to fragmentation. In effect, the drag coefficient γ increased as the meteor descended. Most other cases exhibited a decrease of r with increasing atmospheric density ρ which is less than that predicted by theory. If γ were less than unity, but invariant with height, then the experimental points would still be expected to fit the theoretical line. We can explain the progressive departure of the experimental points from the expected line only if γ is continually changing with height. Thus, these results tend to support the values for $\bar{\gamma}$ obtained by Verniani[18] which show a progressive decrease with height. Verniani's values of $\bar{\gamma}$ have been plotted against height in Fig. 42 and we see that they indicate an almost linear variation. These values were obtained from photographic observations of meteors of somewhat smaller magnitude, i.e., brighter, than the radio meteors. Thus an average height for the start of cap formation of about 104 km is not unreasonable. However, since the values of r show a spread of a factor of 10 (assuming the densities δ are all the same), we should expect cap formation to begin over a range of heights extending ± 1 scale height about this mean value.

X. SUMMARY

Observations of five nighttime meteor showers have yielded values for the shower velocities v_o which tend to be higher than the values obtained in other radar observations. We attribute

this to errors associated with the determination of range. Observations of meteors traveling radially toward the radar were made during three of the above showers. These measurements yielded values of the initial meteor velocities v_∞ which are in good agreement with photographic determinations.

The durations of the meteors were interpreted as yielding measures of the over-all trail lengths of the meteors. All of the showers exhibited somewhat larger average trail lengths than those observed for the sporadic meteors, and the Quadrantid and Geminid trails were three times as long. The average heights of these meteor showers (except for the Perseids) showed no striking differences from sporadics traveling at the same velocity. The Perseid shower had an average height noticeably above that of sporadic meteors indicating that Perseid meteors are of low density.

Intensity measurements were used to yield distributions of cross section. These distributions show that there were many more bright meteors associated with the showers than with the sporadics. However, the mass distribution laws obtained from this work are in disagreement with accepted laws, and we are forced to come to the conclusion that the cross sections are not proportional to the meteor masses. Such behavior might be caused by fragmentation.

The meteors observed traveling down the antenna beam provide very accurate values of velocity vs time. Unfortunately, the height of the meteor is less certain because of the finite width of the antenna beam. The variation of velocity vs height has been computed in each case and used to check the observed behavior against that expected for a meteor which decelerates without forming an air cap. In some cases, good agreement was observed between theory and observation, although in many other cases it was evident that an air cap had formed. An average mass of $10^{-2} - 10^{-3}$ gm was estimated assuming a density of 1 gm/cm^3. This would be consistent with +5 visual magnitude meteors assuming that zero magnitude solid particle meteors have masses in the range 1 to 10^{-1} gm[5]. The scatter in values for the mass was large implying a distribution of about ±3 visual magnitudes.

XI. CONCLUSION

Perhaps the most interesting results obtained during the course of the meteor studies described in this and the previous report[1] are those of meteor velocity vs time found from the radial measurements. No previous reports of meteors observed traveling radially toward the radar have been published. It is most unfortunate that these results could not be used to yield accurate mass values. However, the principal requirement for these observations is that the elevation of the radiant be low. Evidently, simultaneous photographic observations would require a number of wide-angle cameras distributed in an area beneath the intersection of the beam with the meteor region. Such combined observations could yield accurate values of mass, thence the density and radius would also be known. Since the velocity would be determined by the radar, the cameras need not have rotating shutters and could be relatively simple. Such a program would require considerably more effort than was involved in running the radar equipment and consequently could not be entertained.

The need for simultaneous measurements of this type is evident from the results presented herein, which show that free molecular flow does not always take place. Thus, the drag coefficient γ enters the equations as a third unknown quantity. Both γ and the equivalent radius are height dependent. Therefore, unless additional theoretical constraints are introduced, it is not possible to separate variations of one from the other.

ACKNOWLEDGMENTS

We are indebted to G. H. Pettengill and V. C. Pineo for stimulating our interest in this work, and to other members of the staff of Millstone Radar Observatory who have assisted in setting up the equipment for these observations. Helpful discussions have been held with G. S. Hawkins and T. Hafgors.

REFERENCES

1. J. V. Evans and R. A. Brockelman, "Radio-Echo Studies of Meteors at 68-cm Wavelength, Part I: Sporadic Meteors," Technical Report 332 [U], Lincoln Laboratory, M. I. T. (29 October 1963).
2. A. C. B. Lovell, Meteor Astronomy (Clarendon Press, Oxford, 1954).
3. G. H. Pettengill, J. Geophys. Research 67, 409 (1962).
4. R. H. Brown and A. C. B. Lovell, The Exploration of Space by Radio (Wiley, New York, 1958), p. 139.
5. D. W. R. McKinley, Meteor Science and Engineering (McGraw-Hill, New York, 1961).
6. G. S. Hawkins and M. Almond, Mon. Not. Roy. Ast. Soc. 112, 219 (1952).
7. F. L. Whipple and G. S. Hawkins, Handbuch der Physik (Springer-Verlag, Berlin, 1959), Vol. 52.
8. G. S. Hawkins and R. B. Southworth, Smith. Contrib. Astrophys. 2, 349 (1958).
9. T. R. Kaiser, Advances in Physics 2, 495 (1953).
10. I. C. Browne, K. Bullough, S. Evans and T. R. Kaiser, Proc. Phys. Soc. (London) B 69, 83 (1956).
11. A. A. Weiss, Australian J. Phys. 14, 102 (1961).
12. P. C. Fritsch, "Final Technical Report – Antenna and RF Circuit Design – Millstone Hill Radar," Technical Report 193 [U], Lincoln Laboratory, M. I. T. (7 January 1959), DDC 221688.
13. F. L. Whipple and L. G. Jacchia, Smith. Contrib. Astrophys. 1, 183 (1957).
14. F. L. Whipple, Revs. Modern Phys. 15, 246 (1943).
15. F. Verniani, Nuovo cimento 19, 415 (1961).
16. E. J. Öpik, Physics of Meteor Flight in the Atmosphere (Interscience, New York, 1958).
17. U. S. Standard Atmosphere, 1962 (U. S. Government Printing Office, Washington, 1962).
18. F. Verniani, Nuovo cimento 26, 209 (1962).
19. F. L. Whipple, Astron. J. 59, 201 (1954).
20. L. G. Jacchia, Smith. Contrib. Astrophys. 2, 181 (1958).
21. L. G. Jacchia, Astrophys. J. 121, 521 (1955).

APPENDIX
HEAD-ON METEORS

TABLE A-I

GEMINIDS

Height ($km \times 10^{-4}$)	Atmospheric Density ($gm/cm^3 \times 10^{-7}$)	Velocity ($km/sec \times 10^{-2}$)	$r\delta$ ($gm/cm^2 \times 10^{-1}$)
	Number 2		
+.01021391	+.00253975	-.35617995	+.00894069
+.01015359	+.00289398	-.35589998	+.00916004
+.01009333	+.00319910	-.35557997	+.00892639
+.01003313	+.00353550	-.35521996	+.00904083
+.00997316	+.00404185	-.35483998	+.00747203
+.00991326	+.00448435	-.35419994	+.00878810
+.00985348	+.00497281	-.35387998	+.01061916
+.00979369	+.00570195	-.35332000	+.00889778
+.00973427	+.00635075	-.35267996	+.00883102
+.00967484	+.00706982	-.35197997	+.00875473
+.00961571	+.00786507	-.35117995	+.00855445
+.00955665	+.00909227	-.35027998	+.00889778
+.00949794	+.01015871	-.34929996	+.00893115
+.00943928	+.01134568	-.34819996	+.00896930
+.00938093	+.01313602	-.34700000	+.00920295
+.00932270	+.01474452	-.34561997	+.00891208
+.00926518	+.01651740	-.34403997	+.00866889
+.00920742	+.01850938	-.34223997	+.00813007
+.00915050	+.02105188	-.34003996	+.00800132
+.00909364	+.02360337	-.33767998	+.00761508
+.00964832*	+.33684855†		+.00876569‡
	Number 4		
+.00974369	+.00624346	-.36031997	+.01104831
+.00968289	+.00696802	-.35969996	+.01056194
+.00962251	+.00776928	-.35903996	+.01071929
+.00956207	+.00899928	-.35829997	+.01154899
+.00950193	+.01008248	-.35753995	+.01193523
+.00944179	+.01129233	-.35667997	+.01170635
+.00938212	+.01310485	-.35569995	+.01242160
+.00932246	+.01475149	-.35468000	+.01287460
+.00926321	+.01658159	-.35354000	+.01274585
+.00920391	+.01863813	-.35223996	+.01256465
+.00914520	+.02127832	-.35077995	+.01266479
+.00908648	+.02394473	-.34913998	+.01294612
+.00902843	+.02690207	-.34739995	+.01328945
+.00897049	+.03019505	-.34547996	+.01316547
+.00891315	+.03389745	-.34329998	+.01338958
+.00885576	+.03803968	-.34099996	+.01326560
+.00879943	+.04252171	-.33829998	+.01303195
+.00926619*	+.33528929†		+.01234596‡

* Mean height.

† Mean $\cos\chi$.

‡ Mean $r\delta$.

TABLE A-I (Continued)

Height ($km \times 10^{-4}$)	Atmospheric Density ($gm/cm^3 \times 10^{-7}$)	Velocity ($km/sec \times 10^{-2}$)	$r\delta$ ($gm/cm^2 \times 10^{-1}$)
		Number 6	
+.00914120	+.02145034	-.36661994	+.14405727
+.00910997	+.02284163	-.36647999	+.14372825
+.00907891	+.02431130	-.36629998	+.12215137
+.00904786	+.02587395	-.36607998	+.11304378
+.00901687	+.02753317	-.36583995	+.10643005
+.00898587	+.02926784	-.36555999	+.09775161
+.00895512	+.03114897	-.36523997	+.08889675
+.00892436	+.03314167	-.36485999	+.07339000
+.00889378	+.03524339	-.36433994	+.06748199
+.00886309	+.03748404	-.36381995	+.06256103
+.00883269	+.03984189	-.36315000	+.05472183
+.00880223	+.04235267	-.36237996	+.04900932
+.00877213	+.04494816	-.36144995	+.04343032
+.00874179	+.04779189	-.36034995	+.03771305
+.00871199	+.05074954	-.35898000	+.03018856
+.00868201	+.05390292	-.35709995	+.02017498
+.00891000*	+.16828167†		+.07842063‡
		Number 9	
+.01076716	+.00101828	-.36754995	+.01717090
+.01071387	+.00110226	-.36747997	+.01486301
+.01066058	+.00119304	-.36739999	+.01207351
+.01060724	+.00129133	-.36727994	+.00934123
+.01055401	+.00144326	-.36711996	+.00810146
+.01050090	+.00156635	-.36691999	+.00752925
+.01044780	+.00169974	-.36669999	+.00728607
+.01039499	+.00190091	-.36644995	+.00695705
+.01034200	+.00206959	-.36614996	+.00660896
+.01028931	+.00225156	-.36581999	+.00645160
+.01023662	+.00244927	-.36544996	+.00584125
+.01018399	+.00275087	-.36497998	+.00549793
+.01013153	+.00300222	-.36444997	+.00528335
+.01007926	+.00327473	-.36384999	+.00519275
+.01002717	+.00357067	-.36319994	+.00494003
+.00997495	+.00402933	-.36241996	+.00490665
+.00992310	+.00440859	-.36157995	+.00462055
+.00987136	+.00482141	-.36054998	+.00431060
+.00981992	+.00526976	-.35939997	+.00416755
+.00976854	+.00596863	-.35809999	+.00409603
+.00971758	+.00654512	-.35659998	+.00358104
+.00966674	+.00717395	-.35461997	+.00314712
+.00961649	+.00785410	-.35229998	+.00288009
+.00956630	+.00892740	-.34954994	+.00264644
+.00951707	+.00979858	-.34611999	+.00212192
+.01013511*	+.28763699†		+.00638478‡

* Mean height.

† Mean $\cos\chi$.

‡ Mean $r\delta$.

TABLE A-I (Continued)

Height ($km \times 10^{-4}$)	Atmospheric Density ($gm/cm^3 \times 10^{-7}$)	Velocity ($km/sec \times 10^{-2}$)	$r\delta$ ($gm/cm^2 \times 10^{-1}$)
		Number 11	
+.01000463	+.00370675	-.36777997	+.00883102
+.00996768	+.00408059	-.36634999	+.00415325
+.00993072	+.00435072	-.36579996	+.00817298
+.00989395	+.00463670	-.36527997	+.00857353
+.00985747	+.00493860	-.36471998	+.00894069
+.00982093	+.00526052	-.36417996	+.00934123
+.00978451	+.00579798	-.36359995	+.00934600
+.00974822	+.00619250	-.36294996	+.00956058
+.00971198	+.00661170	-.36231994	+.01026153
+.00967586	+.00705695	-.36167997	+.01047611
+.00963997	+.00752854	-.36100000	+.01064300
+.00960415	+.00803071	-.36029994	+.01077175
+.00956845	+.00889110	-.35954999	+.01149177
+.00953280	+.00951170	-.35879999	+.01224994
+.00949728	+.01017129	-.35804998	+.01263141
+.00946187	+.01087307	-.35724997	+.01244544
+.00942677	+.01161634	-.35637998	+.01250267
+.00939154	+.01286101	-.35547995	+.01333713
+.00935661	+.01378673	-.35454994	+.01419067
+.00932180	+.01477062	-.35364997	+.01457691
+.00928711	+.01581794	-.35264998	+.01424789
+.00925260	+.01693212	-.35157996	+.01493930
+.00921821	+.01811987	-.35054999	+.01588344
+.00918406	+.01967018	-.34947997	+.01600742
+.00914990	+.02107721	-.34829998	+.01599311
+.00911599	+.02256691	-.34707999	+.01631259
+.00908219	+.02415186	-.34579998	+.01616477
+.00904864	+.02583378	-.34439998	+.01639842
+.00901526	+.02762216	-.34299999	+.01691341
+.00898206	+.02949541	-.34151995	+.01665115
+.00894898	+.03153747	-.33989995	+.01625061
+.00891607	+.03369885	-.33814996	+.01559734
+.00888365	+.03596806	-.33619999	+.01502513
+.00885123	+.03838711	-.33409994	+.01402378
+.00881922	+.04093343	-.33161997	+.01310348
+.00878733	+.04358243	-.32894998	+.01214981
+.00875592	+.04644769	-.32580000	+.01120567
+.00936472*	+.19688838†		+.01268565‡

* Mean height.

† Mean cos χ.

‡ Mean $r\delta$.

TABLE A-I (Continued)

Height ($km \times 10^{-4}$)	Atmospheric Density ($gm/cm^3 \times 10^{-7}$)	Velocity ($km/sec \times 10^{-2}$)	$r\delta$ ($gm/cm^2 \times 10^{-1}$)
	Number 13		
+.01067739	+.00116360	-.36947995	+.00528335
+.01062208	+.00126320	-.36924999	+.00516891
+.01056665	+.00141543	-.36897999	+.00577926
+.01051151	+.00154095	-.36874997	+.00592231
+.01045644	+.00167727	-.36844998	+.00542163
+.01040130	+.00182580	-.36811995	+.00570774
+.01034641	+.00205498	-.36779999	+.00595569
+.01029145	+.00224381	-.36741995	+.00553607
+.01023685	+.00244832	-.36697995	+.00536918
+.01018220	+.00275909	-.36649996	+.00566959
+.01012772	+.00302135	-.36599999	+.00577926
+.01007330	+.00330734	-.36544996	+.00561237
+.01001906	+.00361901	-.36481994	+.00555515
+.00996500	+.00409966	-.36414998	+.00574111
+.00991100	+.00450193	-.36339998	+.00546932
+.00985717	+.00494110	-.36251997	+.00546455
+.00980371	+.00541949	-.36161994	+.00546932
+.00975024	+.00616985	-.36057996	+.00536918
+.00969702	+.00679266	-.35937994	+.00510692
+.00964397	+.00747454	-.35799998	+.00481128
+.00959151	+.00850981	-.35639995	+.00452041
+.00953900	+.00940090	-.35441994	+.00393390
+.01010322*	+.29743909†		+.00539308‡

* Mean height.

† Mean cos χ.

‡ Mean $r\delta$.

TABLE A-II

QUADRANTIDS

Height ($km \times 10^{-4}$)	Atmospheric Density ($gm/cm^3 \times 10^{-7}$)	Velocity ($km/sec \times 10^{-2}$)	$r\delta$ ($gm/cm^2 \times 10^{-1}$)
		Number 1	
+.01058167	+.00138294	-.42379999	+.00400543
+.01052439	+.00151073	-.42331999	+.00427722
+.01046723	+.00164967	-.42284995	+.00456333
+.01041018	+.00180101	-.42234998	+.00467777
+.01035332	+.00203239	-.42181998	+.00492572
+.01029658	+.00222551	-.42124998	+.00493526
+.01023995	+.00243622	-.42061996	+.00509262
+.01018351	+.00275307	-.41997998	+.00572681
+.01012730	+.00302344	-.41934996	+.00599384
+.01007109	+.00331944	-.41864997	+.00609874
+.01001518	+.00364238	-.41791999	+.00649452
+.00995922	+.00414103	-.41718000	+.00627994
+.00990372	+.00455898	-.41619998	+.00739574
+.00984817	+.00501859	-.41557997	+.00866889
+.01021295*	+.26869940†		+.00565272‡
		Number 2	
+.01095551	+.00071299	-.42601996	+.00971317
+.01091212	+.00075519	-.42589998	+.00685214
+.01086878	+.00079977	-.42571997	+.00620841
+.01082563	+.00084680	-.42554998	+.00575065
+.01078248	+.00099533	-.42531996	+.00574111
+.01073950	+.00106108	-.42508000	+.00552177
+.01069658	+.00113093	-.42479997	+.00527858
+.01065373	+.00120520	-.42449998	+.00525474
+.01061099	+.00128412	-.42417997	+.00509262
+.01056843	+.00141149	-.42381995	+.00520706
+.01052588	+.00150728	-.42344999	+.00526428
+.01048344	+.00160902	-.42304998	+.00539779
+.01044112	+.00171732	-.42264997	+.00554084
+.01039886	+.00188910	-.42221999	+.00560760
+.01035684	+.00202095	-.42174994	+.00572681
+.01031482	+.00216156	-.42127996	+.00575065
+.01063340*	+.20149278†		+.00586926‡

* Mean height.

† Mean $\cos \chi$.

‡ Mean $r\delta$.

TABLE A-II (Continued)

Height ($km \times 10^{-4}$)	Atmospheric Density ($gm/cm^3 \times 10^{-7}$)	Velocity ($km/sec \times 10^{-2}$)	$r\delta$ ($gm/cm^2 \times 10^{-1}$)
	Number 3		
+.00893467	+.03246051	-.43301999	+.60778617
+.00889706	+.03501200	-.43294996	+.49212455
+.00885939	+.03776311	-.43281996	+.39353370
+.00882184	+.04071861	-.43267995	+.42330741
+.00878447	+.04383665	-.43254995	+.40984630
+.00874710	+.04728293	-.43237996	+.33176422
+.00870978	+.05097526	-.43214994	+.33211231
+.00867265	+.05492597	-.43194997	+.34109115
+.00863564	+.05916422	-.43169999	+.33052444
+.00859862	+.06363421	-.43144994	+.35538673
+.00856173	+.06858783	-.43119996	+.36044597
+.00852501	+.07386720	-.43092000	+.34246444
+.00848829	+.07953363	-.43059998	+.33030986
+.00845164	+.08561486	-.43024998	+.36661624
+.00841498	+.09215778	-.42994999	+.38143634
+.00837868	+.09901529	-.42957997	+.36469936
+.00834238	+.10657048	-.42919999	+.36867141
+.00830602	+.11467897	-.42877995	+.37189006
+.00827008	+.12328064	-.42834997	+.38523674
+.00859999*	+.17128628†		+.38364440‡

* Mean height.

† Mean $\cos\chi$.

‡ Mean $r\delta$.

TABLE A-II (Continued)

Height ($km \times 10^{-4}$)	Atmospheric Density ($gm/cm^3 \times 10^{-7}$)	Velocity ($km/sec \times 10^{-2}$)	$r\delta$ ($gm/cm^2 \times 10^{-1}$)
	Number 4		
+.01032388	+.00213044	-.42401999	+.01220703
+.01028293	+.00227457	-.42377996	+.01134395
+.01024204	+.00242811	-.42347997	+.01090049
+.01020115	+.00259202	-.42317998	+.01105785
+.01016050	+.00286084	-.42284995	+.01162052
+.01011991	+.00306081	-.42251998	+.01223564
+.01007938	+.00327408	-.42217999	+.01214504
+.01003909	+.00350064	-.42179995	+.01195907
+.00999879	+.00386542	-.42139995	+.01286029
+.00995868	+.00414484	-.42100000	+.01342296
+.00991863	+.00444287	-.42057996	+.01339435
+.00987863	+.00476115	-.42012000	+.01353740
+.00983887	+.00509989	-.41964995	+.01347541
+.00979900	+.00564718	-.41911995	+.01118659
+.00975948	+.00606745	-.41832000	+.01486778
+.00971996	+.00651705	-.41804999	+.01895427
+.00968068	+.00699573	-.41741997	+.01437664
+.00964140	+.00750917	-.41677999	+.01461029
+.00960218	+.00805920	-.41607999	+.01496791
+.0095314	+.00898098	-.41538000	+.01546859
+.00952440	+.00966387	-.41457998	+.01556873
+.00948554	+.01039892	-.41377997	+.01569747
+.00944709	+.01118004	-.41288000	+.01479148
+.00940859	+.01202094	-.41184997	+.01436710
+.00937032	+.01341640	-.41074997	+.01543521
+.00933218	+.01447075	-.40964996	+.01562118
+.00929433	+.01559442	-.40841996	+.01561164
+.00925642	+.01680523	-.40714997	+.01594066
+.00921899	+.01809221	-.40579998	+.01565456
+.00918155	+.01977038	-.40429997	+.01554012
+.00914436	+.02131414	-.40267997	+.01515388
+.00910741	+.02295958	-.40087997	+.01406192
+.00907075	+.02471292	-.39874994	+.01300811
+.00903421	+.02659195	-.39634996	+.01203060
+.00899821	+.02854233	-.39354997	+.01060485
+.00964808*	+.18818366†		+.01381939‡

*Mean height.

†Mean $\cos\chi$.

‡Mean $r\delta$.

TABLE A-II (Continued)

Height ($km \times 10^{-4}$)	Atmospheric Density ($gm/cm^3 \times 10^{-7}$)	Velocity ($km/sec \times 10^{-2}$)	$r\delta$ ($gm/cm^2 \times 10^{-1}$)
		Number 5	
+.01099509	+.00067651	-.42779999	+.00686645
+.01095247	+.00071585	-.42764997	+.00699996
+.01090979	+.00075751	-.42751997	+.00692367
+.01086717	+.00080150	-.42734998	+.00645637
+.01082468	+.00084787	-.42717999	+.00627994
+.01078218	+.00099575	-.42697995	+.00632762
+.01073998	+.00106030	-.42675000	+.00602245
+.01069778	+.00112891	-.42649996	+.00580787
+.01065570	+.00120168	-.42621999	+.00629425
+.01061362	+.00127917	-.42597997	+.00644207
+.01057171	+.00140434	-.42567998	+.00605583
+.01052981	+.00149816	-.42534995	+.00597953
+.01048809	+.00159758	-.42499995	+.00576496
+.01044648	+.00170320	-.42460000	+.00575065
+.01040500	+.00181543	-.42419999	+.00576496
+.01036351	+.00199943	-.42374998	+.00585556
+.01032221	+.00213617	-.42328000	+.00604152
+.01028096	+.00228178	-.42280000	+.00594139
+.01023989	+.00243645	-.42224997	+.00565528
+.01019906	+.00268232	-.42164999	+.00595092
+.01015818	+.00287193	-.42104995	+.00587940
+.01011741	+.00307357	-.42034995	+.00581264
+.01007694	+.00328743	-.41964995	+.00590801
+.01003640	+.00351631	-.41887998	+.00577926
+.00999623	+.00388276	-.41804999	+.00605106
+.00995600	+.00416421	-.41719996	+.00556945
+.00991606	+.00446265	-.41609996	+.00493526
+.00987613	+.00478184	-.41484999	+.00489711
+.00983655	+.00512045	-.41358000	+.00486373
+.00979709	+.00566679	-.41214996	+.00483989
+.00975787	+.00608515	-.41059994	+.00480651
+.00971889	+.00652968	-.40894997	+.00467777
+.00968009	+.00700330	-.40709996	+.00452041
+.00964158	+.00750672	-.40509998	+.00433921
+.00960332	+.00804281	-.40284997	+.00391960
+.00956517	+.00894659	-.40009999	+.00358104
+.00952762	+.00960534	-.39684998	+.00319004
+.00949031	+.01030588	-.39299994	+.00269412
+.01022726*	+.19422733†		+.00551176‡

*Mean height.

†Mean $\cos \chi$.

‡Mean $r\delta$.

TABLE A-II (Continued)

Height ($km \times 10^{-4}$)	Atmospheric Density ($gm/cm^3 \times 10^{-7}$)	Velocity ($km/sec \times 10^{-2}$)	$r\delta$ ($gm/cm^2 \times 10^{-1}$)
	Number 7		
+.01087695	+.00079119	-.42199999	+.00556468
+.01082795	+.00084418	-.42181998	+.00592708
+.01077896	+.00100058	-.42161995	+.00666618
+.01073014	+.00107592	-.42141997	+.00609397
+.01068139	+.00115674	-.42114996	+.00615119
+.01063269	+.00124347	-.42091995	+.00702857
+.01058411	+.00137770	-.42067998	+.00702381
+.01053565	+.00148469	-.42039996	+.00656604
+.01048713	+.00159990	-.42007994	+.00705718
+.01043891	+.00172311	-.41979998	+.00722408
+.01039069	+.00191408	-.41944998	+.00701427
+.01034259	+.00206762	-.41907995	+.00707149
+.01029461	+.00223255	-.41867995	+.00733852
+.01024675	+.00240993	-.41828000	+.00761032
+.01019906	+.00268232	-.41784995	+.00780105
+.01015132	+.00290495	-.41737997	+.00799655
+.01010382	+.00314384	-.41689997	+.00836849
+.01005631	+.00340193	-.41639995	+.00841140
+.01000922	+.00367861	-.41584998	+.00828742
+.00996196	+.00412136	-.41525000	+.00910282
+.00991505	+.00447046	-.41468000	+.00936985
+.00986802	+.00484931	-.41402000	+.00917434
+.00982129	+.00525730	-.41332000	+.00935554
+.00977462	+.00590312	-.41257995	+.00977516
+.00972825	+.00642019	-.41177999	+.00971317
+.00968188	+.00698071	-.41089999	+.00949859
+.00963580	+.00758540	-.40991997	+.00932693
+.00958973	+.00853878	-.40884995	+.00963211
+.00954413	+.00931024	-.40770000	+.00939846
+.00949835	+.01015073	-.40637999	+.00892639
+.00945305	+.01105523	-.40487998	+.00867366
+.00940793	+.01203578	-.40324997	+.00808238
+.00936311	+.01361006	-.40125000	+.00782966
+.00931841	+.01487016	-.39904999	+.00771522
+.00927430	+.01622295	-.39664995	+.00757217
+.00923025	+.01769489	-.39399999	+.00748634
+.00918686	+.01955866	-.39114999	+.00741481
+.00914353	+.02135002	-.38794994	+.00724315
+.00910097	+.02325838	-.38449996	+.00701427
+.00905847	+.02532917	-.38059997	+.00691413
+.00901693	+.02752989	-.37654995	+.00609874
+.00992536*	+.22661244†		+.00781750‡

*Mean height.

†Mean $\cos\chi$.

‡Mean $r\delta$.

TABLE A-II (Continued)

Height ($km \times 10^{-4}$)	Atmospheric Density ($gm/cm^3 \times 10^{-7}$)	Velocity ($km/sec \times 10^{-2}$)	$r\delta$ ($gm/cm^2 \times 10^{-1}$)
	Number 8		
+.01021146	+.00254964	-.43127995	+.01366615
+.01016038	+.00286138	-.43097996	+.01327991
+.01010942	+.00311470	-.43067997	+.01312255
+.01005852	+.00338953	-.43031996	+.01287460
+.01000791	+.00368660	-.42994999	+.01326084
+.00995719	+.00415557	-.42954999	+.01439094
+.00990658	+.00453644	-.42914998	+.01474857
+.00985616	+.00494980	-.42869997	+.01513957
+.00980597	+.00539833	-.42824995	+.01562118
+.00975573	+.00610888	-.42774999	+.01627922
+.00970572	+.00668680	-.42721998	+.01592636
+.00965565	+.00731879	-.42659997	+.01707077
+.00960600	+.00800400	-.42604994	+.01812934
+.00955635	+.00909739	-.42539995	+.01855373
+.00950688	+.00998884	-.42471998	+.01928806
+.00945752	+.01096254	-.42399996	+.01882553
+.00940829	+.01202768	-.42315000	+.01956939
+.00935930	+.01371353	-.42234998	+.02037048
+.00931042	+.01510667	-.42135000	+.01871109
+.00926172	+.01663035	-.42019999	+.01835823
+.00921320	+.01829963	-.41894996	+.01911163
+.00916498	+.02044498	-.41767996	+.01929759
+.00911694	+.02252364	-.41617995	+.01870155
+.00906908	+.02479583	-.41454994	+.01879692
+.00902158	+.02727442	-.41277998	+.01937389
+.00897419	+.02996987	-.41095000	+.01945495
+.00892734	+.03294342	-.40887999	+.01918792
+.00888061	+.03618830	-.40664994	+.01894474
+.00883442	+.03970396	-.40414994	+.01869678
+.00878828	+.04349803	-.40144997	+.01791477
+.00874274	+.04770004	-.39827996	+.01669883
+.00869745	+.05225610	-.39464998	+.01618385
+.00944024*	+.23239564†		+.01717376‡
	Number 9		
+.00951904	+.00976228	-.41101998	+.01545429
+.00947016	+.01070469	-.41017997	+.01484870
+.00942146	+.01173293	-.40919995	+.01383781
+.00937294	+.01334661	-.40805000	+.01343250
+.00932478	+.01468384	-.40671998	+.01286506
+.00927668	+.01614683	-.40521997	+.01169204
+.00922894	+.01774066	-.40331995	+.01103401
+.00918143	+.01977515	-.40129995	+.01104831
+.00913429	+.02175116	-.39899998	+.01034259
+.00908744	+.02389895	-.39627999	+.00944614
+.00904113	+.02622580	-.39304995	+.00825881
+.00927799*	+.23655349†		+.01202362‡

*Mean height.

†Mean cos χ.

‡Mean $r\delta$.

TABLE A-II (Continued)

Height ($km \times 10^{-4}$)	Atmospheric Density ($gm/cm^3 \times 10^{-7}$)	Velocity ($km/sec \times 10^{-2}$)	$r\delta$ ($gm/cm^2 \times 10^{-1}$)
	Number 10		
+.01074665	+.00104981	-.41817998	+.00458240
+.01069468	+.00113415	-.41784995	+.00423908
+.01064258	+.00122535	-.41747999	+.00400543
+.01059079	+.00136357	-.41705000	+.00394821
+.01053899	+.00147712	-.41657996	+.00373363
+.01048737	+.00159931	-.41601997	+.00366687
+.01043593	+.00173103	-.41544997	+.00360965
+.01038450	+.00193327	-.41477996	+.00349044
+.01033329	+.00209861	-.41402000	+.00352382
+.01028215	+.00227743	-.41324996	+.00343322
+.01023137	+.00246989	-.41231995	+.00330924
+.01018059	+.00276654	-.41134995	+.00339031
+.01013022	+.00300878	-.41024994	+.00329494
+.01007980	+.00327181	-.40904998	+.00321865
+.01002973	+.00355547	-.40770000	+.00313282
+.00997990	+.00399482	-.40621995	+.00318050
+.00993037	+.00435346	-.40459996	+.00317573
+.00988090	+.00474256	-.40284997	+.00307559
+.00983196	+.00516122	-.40084999	+.00289440
+.01028484*	+.24676543†		+.00352126‡
	Number 11		
+.01103371	+.00057053	-.42170000	+.00353813
+.01098233	+.00068807	-.42144995	+.00366210
+.01093119	+.00073635	-.42119997	+.00326156
+.01088005	+.00078797	-.42084997	+.00298976
+.01082909	+.00084292	-.42049998	+.00290393
+.01077812	+.00100177	-.42007994	+.00300884
+.01072746	+.00108021	-.41961997	+.00285148
+.01067674	+.00116473	-.41907995	+.00268936
+.01062625	+.00125539	-.41847997	+.00257492
+.01057571	+.00139576	-.41779994	+.00250339
+.01052558	+.00150793	-.41701996	+.00242233
+.01047557	+.00162863	-.41617995	+.00235080
+.01042550	+.00175905	-.41521996	+.00232219
+.01037579	+.00196045	-.41421997	+.00231742
+.01032644	+.00212174	-.41304999	+.00219345
+.01027703	+.00229614	-.41174995	+.00210762
+.01022803	+.00248306	-.41027998	+.00207424
+.01017898	+.00277400	-.40871995	+.00211715
+.01013058	+.00300699	-.40700000	+.00282287
+.01057809*	+.24092602†		+.00266915‡

*Mean height.

†Mean $\cos\chi$.

‡Mean $r\delta$.

TABLE A-II (Continued)

Height ($km \times 10^{-4}$)	Atmospheric Density ($gm/cm^3 \times 10^{-7}$)	Velocity ($km/sec \times 10^{-2}$)	$r\delta$ ($gm/cm^2 \times 10^{-1}$)
	Number 12		
+.01102852	+.00057393	-.41127997	+.00428199
+.01098036	+.00068986	-.41108000	+.00459194
+.01093238	+.00073516	-.41089999	+.00489711
+.01088428	+.00078356	-.41069996	+.00440597
+.01083642	+.00083482	-.41044998	+.00422000
+.01078850	+.00098645	-.41019999	+.00497817
+.01074081	+.00105899	-.40994995	+.00443935
+.01069319	+.00113666	-.40959995	+.00408172
+.01064568	+.00121968	-.40924996	+.00408172
+.01059818	+.00134807	-.40884995	+.00407695
+.01055085	+.00145030	-.40841996	+.00403404
+.01050353	+.00156003	-.40794998	+.00389099
+.01045650	+.00167715	-.40741997	+.00369071
+.01040953	+.00180280	-.40681999	+.00366210
+.01036274	+.00200194	-.40619999	+.00369548
+.01031595	+.00215762	-.40547996	+.00359535
+.01026946	+.00232410	-.40471994	+.00350475
+.01022297	+.00250327	-.40384995	+.00336170
+.01017689	+.00278365	-.40289998	+.00343799
+.01013070	+.00300639	-.40187996	+.00333786
+.01008492	+.00324410	-.40072000	+.00325202
+.01003903	+.00350099	-.39947998	+.00319480
+.00999367	+.00390011	-.39809995	+.00323772
+.00994831	+.00422012	-.39661997	+.00326156
+.01048302*	+.23114907†		+.00388360‡

*Mean height.

†Mean cos χ.

‡Mean $r\delta$.

TABLE A-II (Continued)

Height ($km \times 10^{-4}$)	Atmospheric Density ($gm/cm^3 \times 10^{-7}$)	Velocity ($km/sec \times 10^{-2}$)	$r\delta$ ($gm/cm^2 \times 10^{-1}$)
		Number 13	
+.01192730	+.00016880	-.41924995	+.00103473
+.01187860	+.00017499	-.41904997	+.00102043
+.01182991	+.00018143	-.41879999	+.00101566
+.01178139	+.00020480	-.41857999	+.00119209
+.01173299	+.00021302	-.41834998	+.00116348
+.01168465	+.00022161	-.41809999	+.00109195
+.01163649	+.00023049	-.41781997	+.00109195
+.01158827	+.00026303	-.41754996	+.00120639
+.01154029	+.00027465	-.41724997	+.00113487
+.01149231	+.00028681	-.41691994	+.00118732
+.01144456	+.00029939	-.41661995	+.00116348
+.01139664	+.00034582	-.41624999	+.00121593
+.01134908	+.00036287	-.41587996	+.00122070
+.01130157	+.00038069	-.41547995	+.00118732
+.01125413	+.00039935	-.41504997	+.00120162
+.01120674	+.00041890	-.41461998	+.00115871
+.01115959	+.00049394	-.41411995	+.00124454
+.01111245	+.00052136	-.41359996	+.00124931
+.01106548	+.00055015	-.41304999	+.00119209
+.01101863	+.00058048	-.41241997	+.00113487
+.01097208	+.00069749	-.41174995	+.00129222
+.01092553	+.00074189	-.41104996	+.00127792
+.01087903	+.00078898	-.41027998	+.00122070
+.01083278	+.00083881	-.40941995	+.00117778
+.01078677	+.00098896	-.40849995	+.00127315
+.01074069	+.00105917	-.40748000	+.00117301
+.01069515	+.00113332	-.40625000	+.00108718
+.01064956	+.00121271	-.40489995	+.00100135
+.01060426	+.00129705	-.40327996	+.00087261
+.01055908	+.00143206	-.40127998	+.00078678
+.01051443	+.00153404	-.39887994	+.00070095
+.01046997	+.00164276	-.39607995	+.00054836
+.01118844*	+.22791469†		+.00111049‡

*Mean height.

†Mean $\cos\chi$.

‡Mean $r\delta$.